Title

Gas Immersion Laser Doping of silicon wafers: Large area n++ phosphorus doping on p++ emitters by laser spot rastering

Authors

Guilherme Gaspar*[a], Afonso F. Guerra*[a], Filipe C. Serra[a], Ana S. Viana[b], Jayaprasad Arumughan[c], Ivo Costa[a], David M. Pêra[a], José A. Silva[a], Lasse Vines[d], João M. Serra[a], Killian Lobato*[a]

Affiliations

[a] Instituto Dom Luiz, Faculdade de Ciências, Universidade de Lisboa; [b] Centro de Química Estrutural, Faculdade de Ciências, Universidade de Lisboa; [c] International Solar Energy Research Centre – ISC Konstanz; [d] Department of Physics, Centre for Materials Science and Nanotechnology, University of Oslo

*Authors contributed in equal measure.

Abstract

Hybrid perovskite-silicon tandem solar cell architectures are currently considered as one of the more promising architectures for the widespread deployment of devices employing 2 junctions. These have the potential to go beyond the single junction Shockley-Queisser limit (ca. 33%). In fact, lab scale devices have already surpassed 29% efficiencies[1], already displacing the current record efficiencies for single junction silicon and perovskite devices.

A range of strategies have been reported to interconnect the bottom silicon sub-cell with the top perovskite sub-cell [2, 3]. Forming a tunnel junction between the sub-cells is one such strategy. The connecting intermediate layer must efficiently transport one type of carrier from each sub-cell, whilst hindering the other carrier type. It must have a high vertical conductivity, but low lateral conductivity to prevent carrier recombination. Additionally, the optical coupling between the two sub-cells is critical to minimise parasitic absorption and unwanted reflectivity.

Here we report on the current status of our approach[4] at forming tunnel junctions directly on the silicon sub-cell using GILD[5]. We believe that this approach is scalable, cost-effective, and simple to integrate into manufacturing lines, unlike tunnel junction formation by ion implantation [6].

In short, our doping system consists of an Nd:YAG ns pulsed 1064nm laser coupled to a high speed galvano head, which permits the rastering of the laser spot over areas up to 10x10 cm2. The wafer samples are held in an argon filled chamber at atmospheric pressure and saturated with phosphorus(V) oxychloride (POCl3). The laser pulse melts a thin (hundreds of nm) layer which quickly incorporates the phosphorus adsorbed at the surface of the wafer before solidifying.

To form n++/p++ tunnelling interfaces we used our system to n++ dope a thin layer on p++ emitters that were already formed on n-type silicon wafers. Laser pulse energy, spot spacing

and pattern, and number of passages are varied and their impact on phosphorus n++ doping profiles is analysed by secondary-ion beam microscopy. Because the surface undergoes melting-solidification cycles, the resultant surface topology is analysed by atomic force microscopy (AFM) and scanning electron microscopy (SEM).

References

1 Green M, et al (2021) Solar cell efficiency tables (version 57). Prog Photovoltaics Res Appl 29:3–15. DOI:10.1002/pip.3371

2 Ko Y, et al (2020) Recent Progress in Interconnection Layer for Hybrid Photovoltaic Tandems. Adv Mater 32:2002196. DOI:10.1002/adma.202002196

3 Jošt M, et al (2020) Monolithic Perovskite Tandem Solar Cells: A Review of the Present Status and Advanced Characterization Methods Toward 30% Efficiency. Adv Energy Mater 10:1904102. DOI:10.1002/aenm.201904102

4 Gaspar G et al (2020) Sequential silicon surface melting and atmospheric pressure phosphorus doping for crystalline tunnel junction formation in silicon/perovskite tandem solar cells. In: 37th EU PVSEC 2020, European PV Solar Energy Conference and Exhibition, Lisbon. DOI:10.4229/EUPVSEC20202020-3BV.2.102

5 Turner GB, et al (1981) Solar cells made by laser-induced diffusion directly from phosphine gas. Appl Phys Lett 39:967–969. DOI:10.1063/1.92628

6 Bellanger P, et al (2018) Silicon Tunnel Junctions Produced by Ion Implantation and Diffusion Processes for Tandem Solar Cells. IEEE J Photovoltaics 8:1436–1442. DOI:10.1109/JPHOTOV.2018.2864632

Mendeley References

1. Green M, Dunlop E, Hohl-Ebinger J, et al (2021) Solar cell efficiency tables (version 57). Prog Photovoltaics Res Appl 29:3–15. https://doi.org/10.1002/pip.3371
2. Ko Y, Park H, Lee C, et al (2020) Recent Progress in Interconnection Layer for Hybrid Photovoltaic Tandems. Adv Mater 32:2002196. https://doi.org/10.1002/adma.202002196
3. Jošt M, Kegelmann L, Korte L, Albrecht S (2020) Monolithic Perovskite Tandem Solar Cells: A Review of the Present Status and Advanced Characterization Methods Toward 30% Efficiency. Adv Energy Mater 10:1904102. https://doi.org/10.1002/aenm.201904102
4. Gaspar G, Cardoso JJ, Costa I, et al (2020) Sequential silicon surface melting and atmospheric pressure phosphorus doping for crystalline tunnel junction formation in silicon/perovskite tandem solar cells. In: 37th EU PVSEC 2020, European PV Solar Energy Conference and Exhibition, Lisbon. Lisbon
5. Turner GB, Tarrant D, Pollock G, et al (1981) Solar cells made by laser-induced

diffusion directly from phosphine gas. Appl Phys Lett 39:967–969. https://doi.org/10.1063/1.92628

6. Bellanger P, Minj A, Fave A, et al (2018) Silicon Tunnel Junctions Produced by Ion Implantation and Diffusion Processes for Tandem Solar Cells. IEEE J Photovoltaics 8:1436–1442. https://doi.org/10.1109/JPHOTOV.2018.2864632

Gas Immersion Laser Doping of silicon wafers:

Large area n++ phosphorus doping on p++ emitters by laser spot rastering

Guilherme Gaspar*[a], Afonso F. Guerra*[a], Filipe C. Serra [a], Ana S. Viana[b], Jayaprasad Arumughan[c], Ivo Costa[a], David M. Pêra[a], José A. Silva[a], Lasse Vines[d], João M. Serra[a], Killian Lobato*[a]

a Instituto Dom Luiz, Faculdade de Ciências, Universidade de Lisboa;
b Centro de Química Estrutural, Faculdade de Ciências, Universidade de Lisboa;
c International Solar Energy Research Centre – ISC Konstanz;
d Department of Physics, Centre for Materials Science and Nanotechnology, University of Oslo

*Presenting authors

The S-LoTTuSS project was supported the Portuguese Science and Technology Foundation (FCT) through the grant agreements PTDC/CTM-CTM/28962/2017, PTDC/CTMCTM/28860/2017, 02/SAICT/2017 Nº 02883, UIDB/00100/2020-CQE and UIDB/50019/2020 – IDL financed by national funds FCT/MCTES (PIDDAC), and supported by The Research Council of Norway (RCN) through Project No. 239895/F20.

Contents

1.1 Perovskite on silicon tandem solar cells

- Why tandem devices?

Device type	Bandgaps (eV)	AM1.5G efficiency (%)
Single junction	1.34	33.68
Double junction	0.94 and 1.73	46.06
Tripe junction	0.93, 1.40eV and 2.05	51.94

Bremner et al. Prog. Photovolt: Res. Appl. 2008; 16:225–233

- Theoretical efficiencies of >45% are possible for a combinational range of top and bottom cell bandgaps of 0.9 to 1.1 eV and 1.55 to 1.75eV respectively.

- Practical efficiencies are estimated to be at 35%

1.1 Perovskite on silicon tandem solar cells

- Tandem devices require an electrical connection between top and bottom cell, so that electrons and holes can be recycled tandem photon absorption.

- The recombination junction allows holes and electrons to recombine at minimal energy loss.

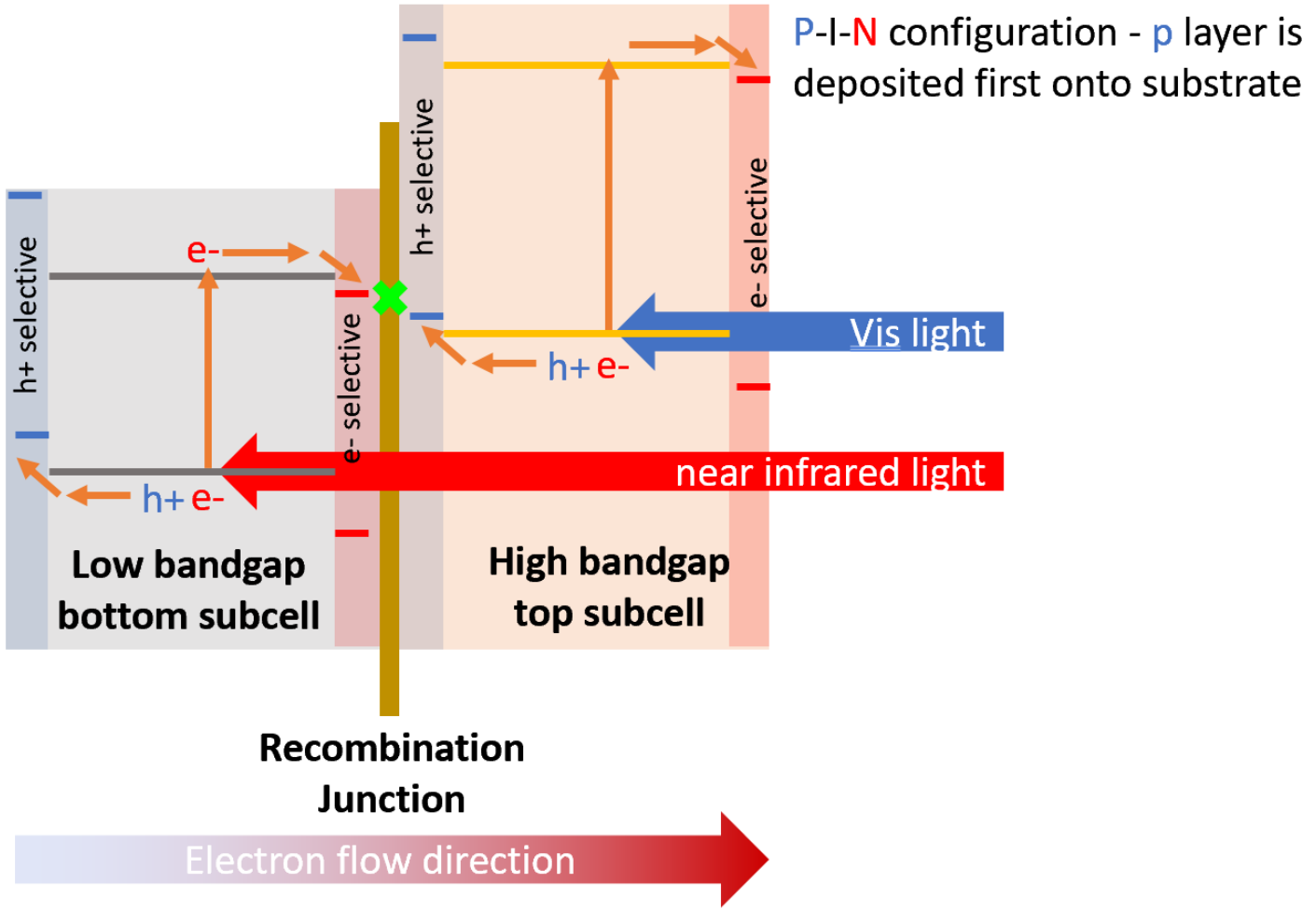

1.1 Perovskite on silicon tandem solar cells

- Current flow is determined by placement of selective contacts.

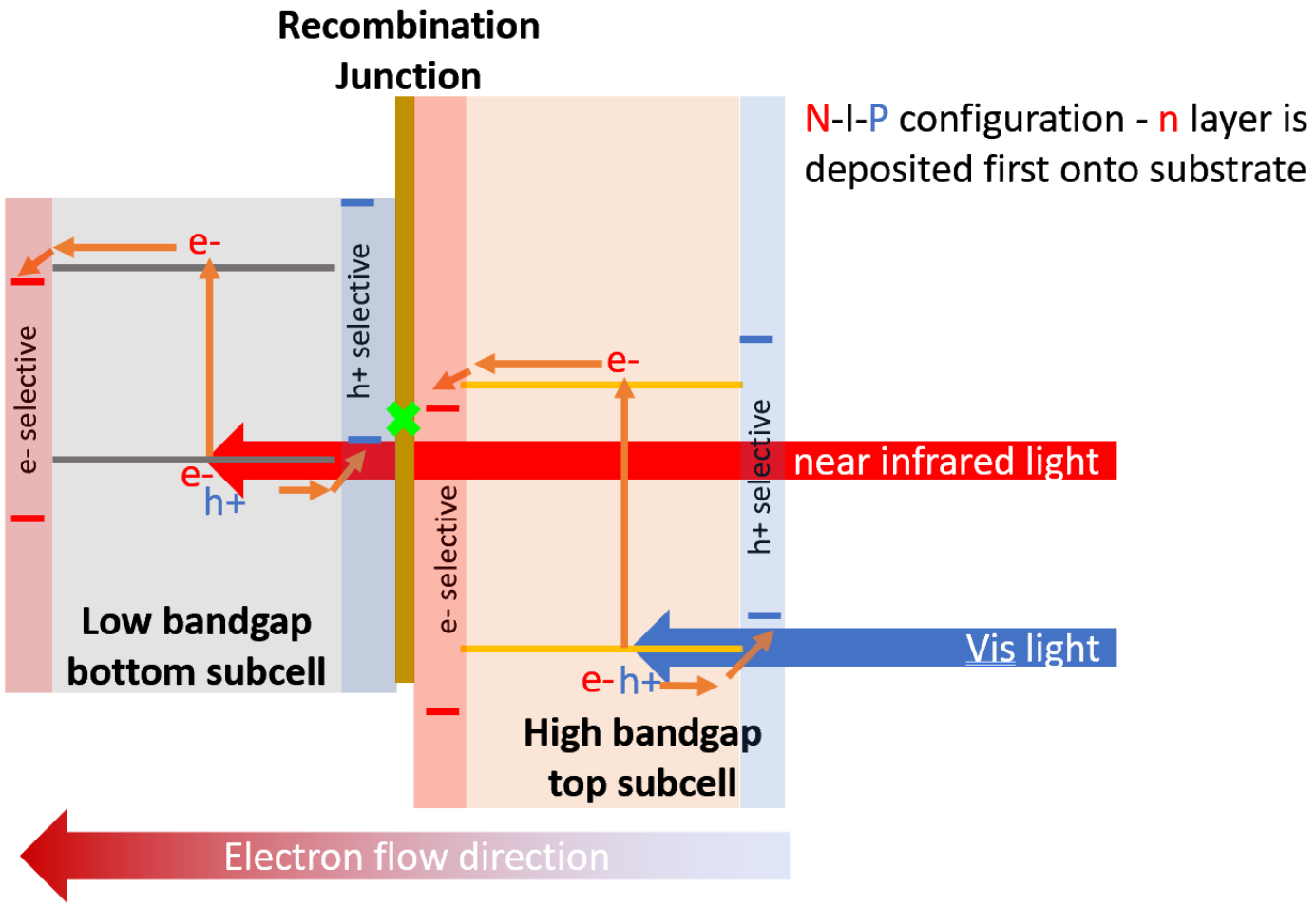

1.1 Perovskite on silicon tandem solar cells

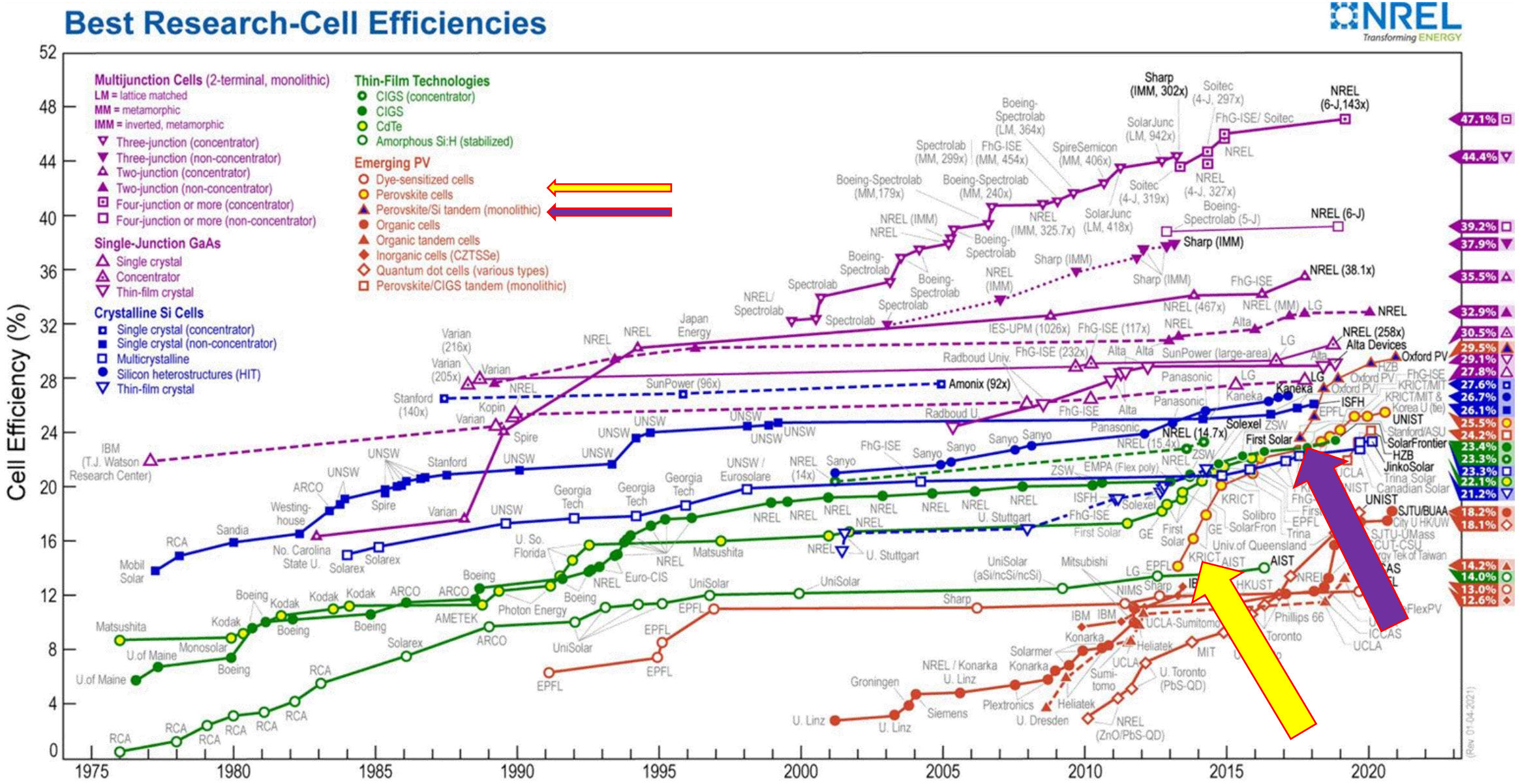

This plot is courtesy of the National Renewable Energy Laboratory, Golden, CO

1.1 Perovskite on silicon tandem solar cells

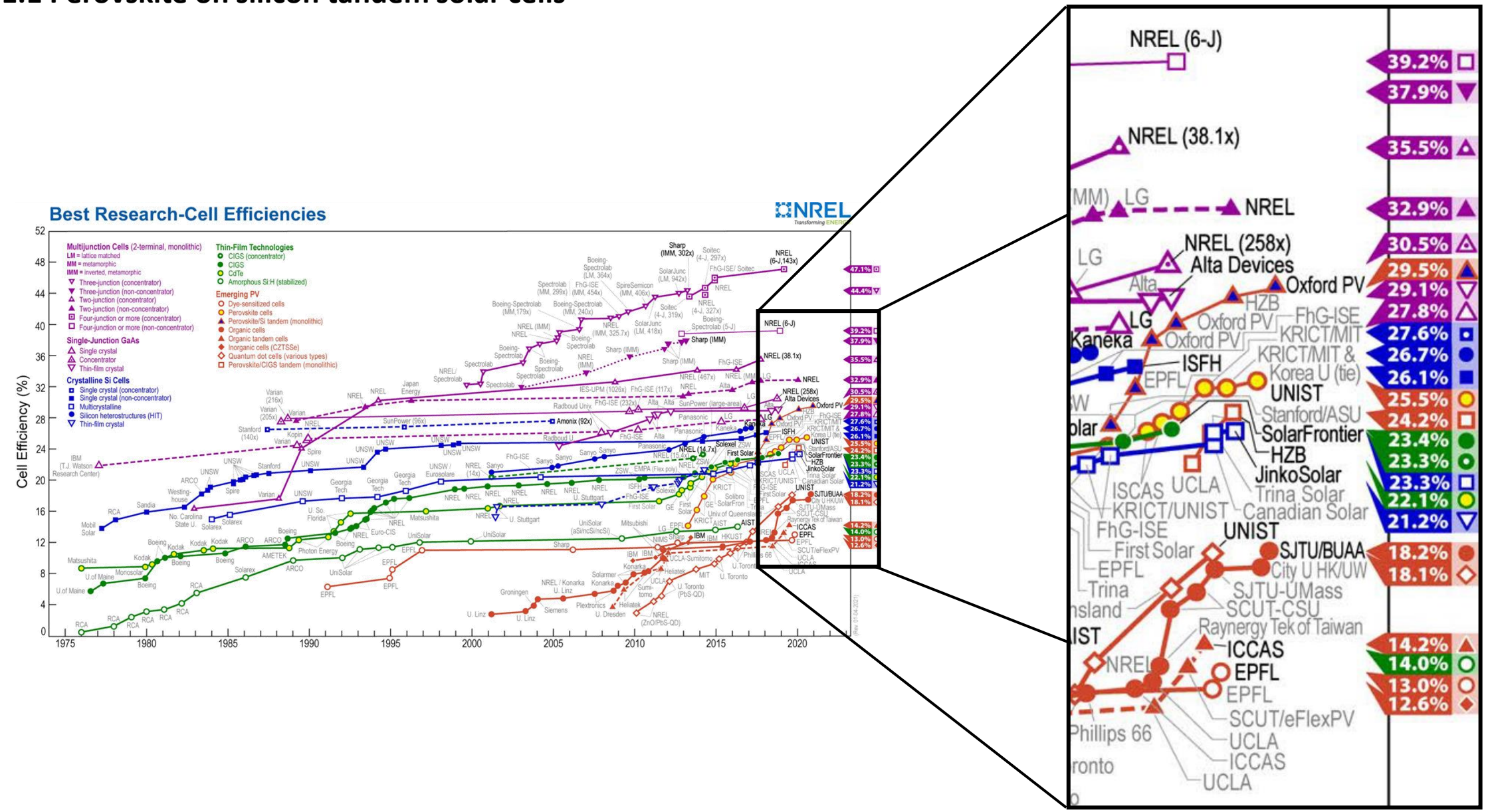

This plot is courtesy of the National Renewable Energy Laboratory, Golden, CO

1.1 Perovskite on silicon tandem solar cells

- Graph shows all reported perovskite on silicon device efficiencies and areas in a 2-terminal monolithic configuration

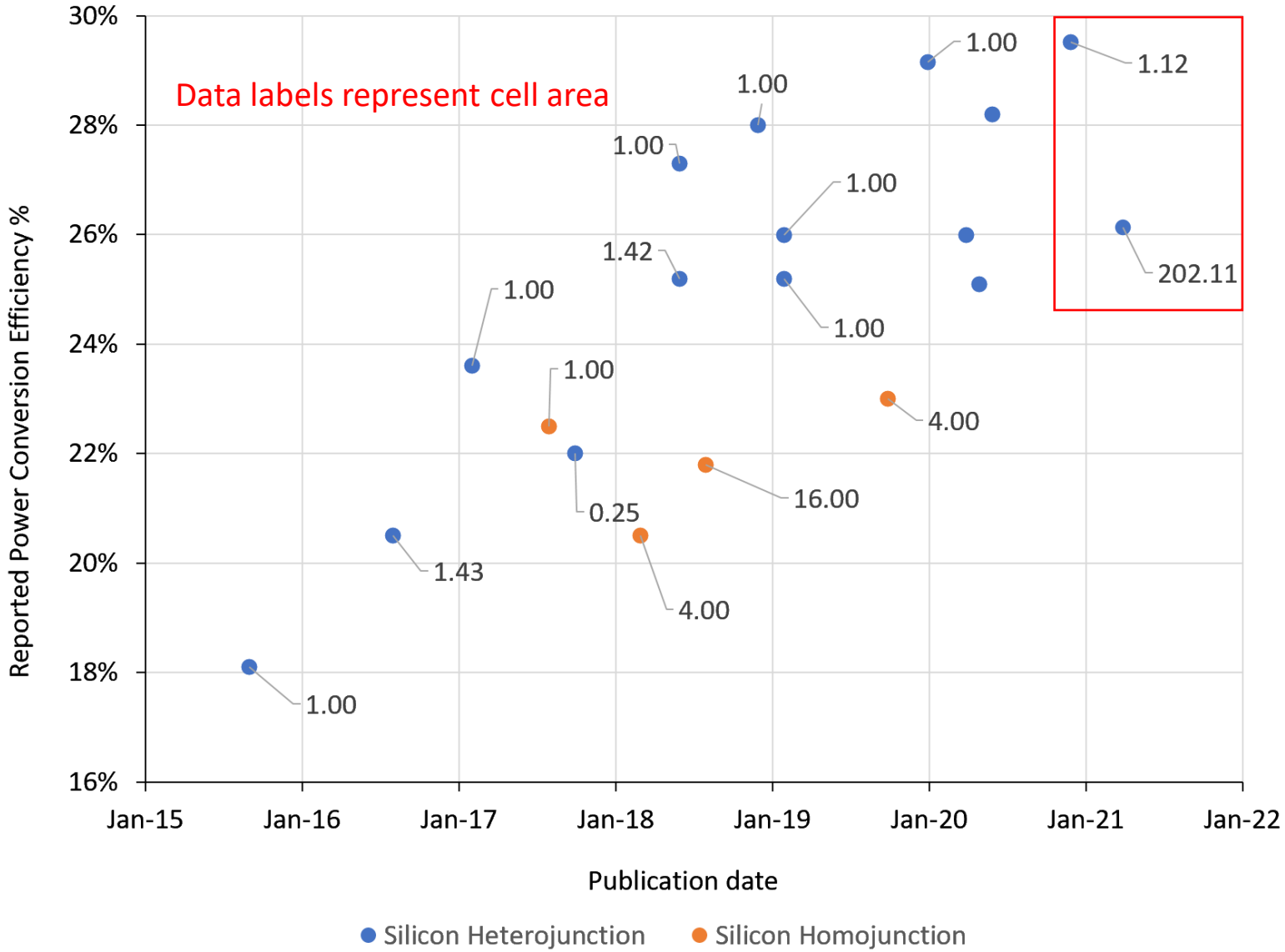

1.1 Perovskite on silicon tandem solar cells

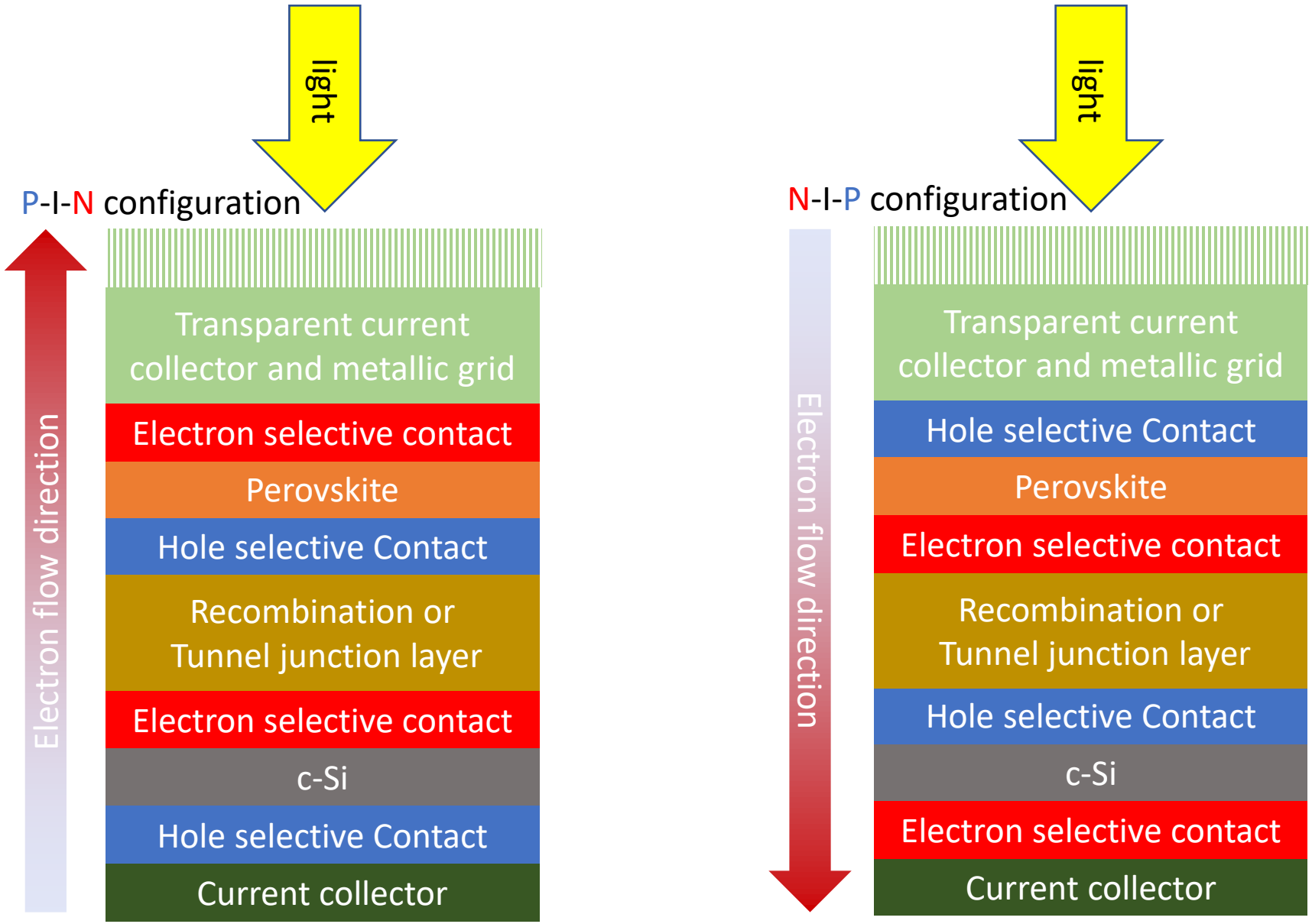

1.1 Perovskite on silicon tandem solar cells

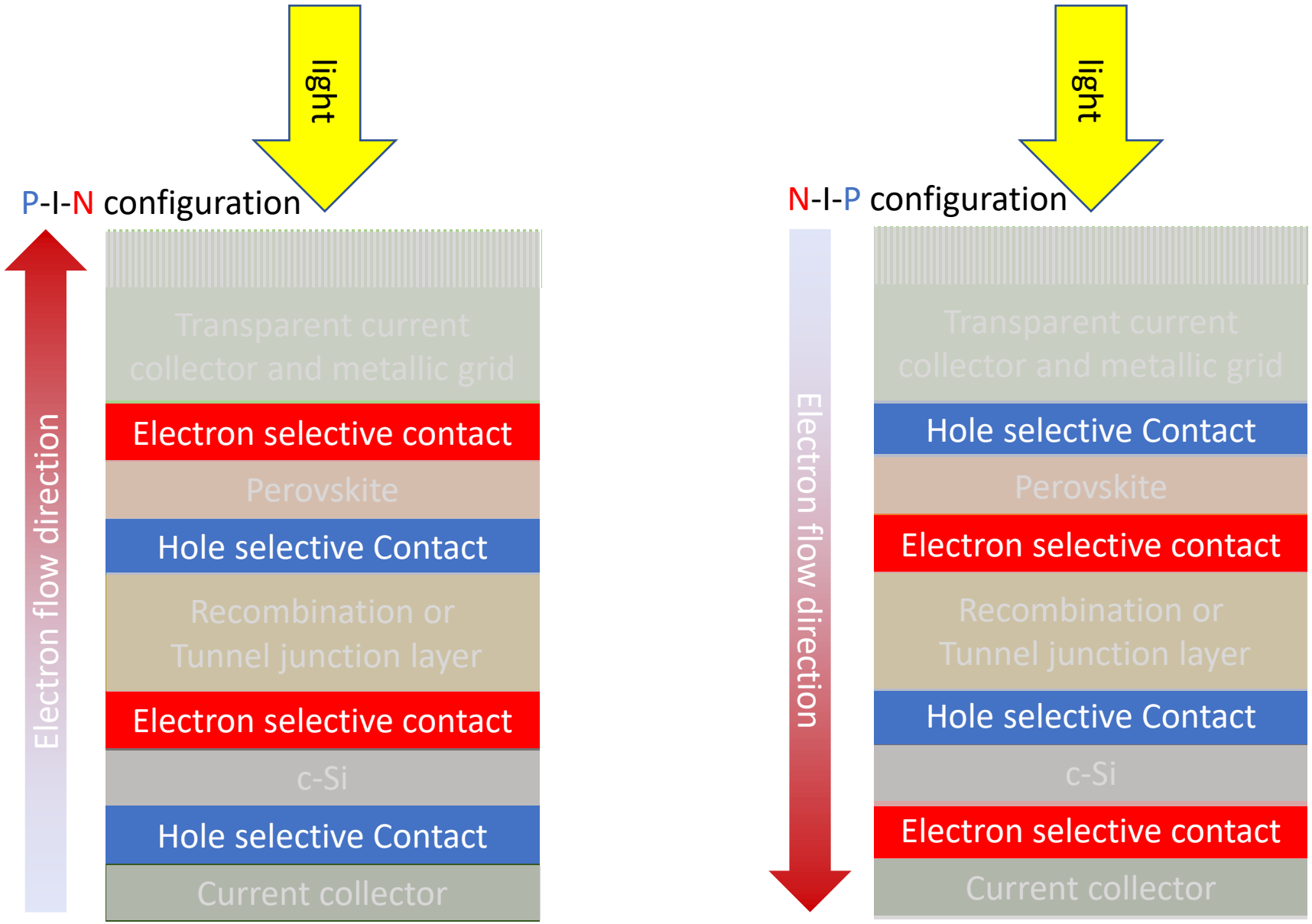

1.1 Perovskite on silicon tandem solar cells

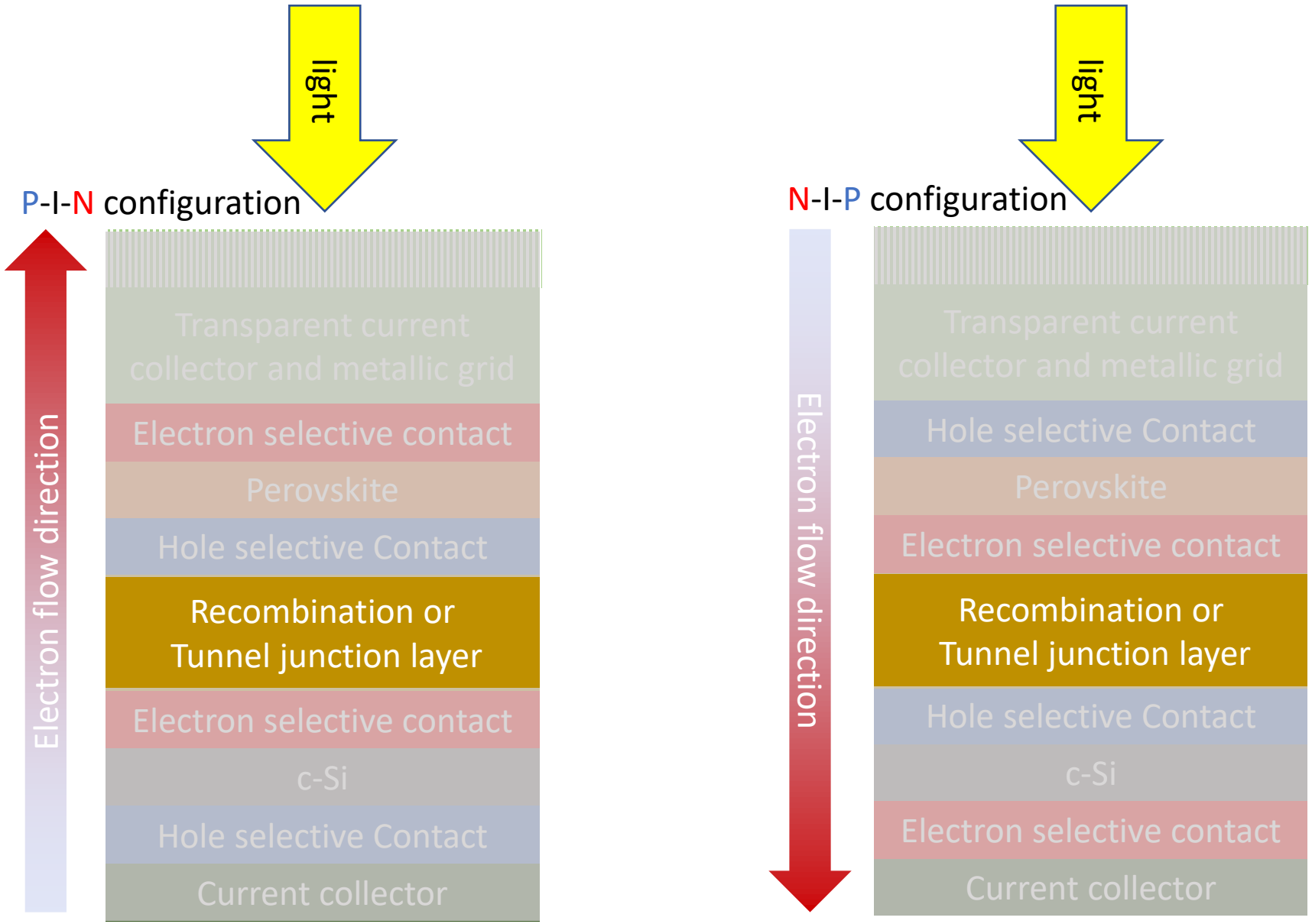

1.1 Perovskite on silicon tandem solar cells

- Strategies for interconnecting the top and bottom subcells are varied
  - Mailoa (2015) *A 2-terminal perovskite/silicon multijunction solar cell enabled by a silicon tunnel junction.* Appl Phys Lett 106:121105.
  - 13.7% efficiency – **homojunction** c-Si subcell
  - Nanocrystalline Si tunnel junction
  - Very poor performance due to lack of optimization of several layers (6 years is a long time in this area).

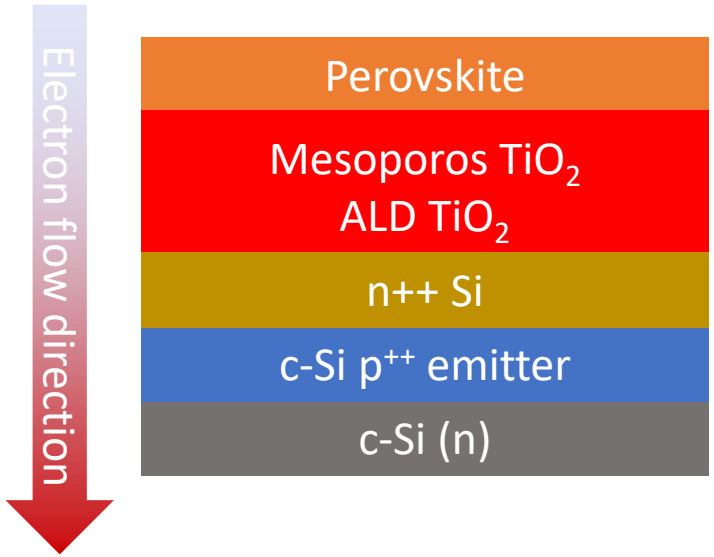

Heavily doped a-Si:H by PECVD and then annealed at 380 deg.C to form nc-Si

1.1 Perovskite on silicon tandem solar cells

- Strategies for interconnecting the top and bottom subcells are varied
  - Albrecht (2016) *Monolithic perovskite/silicon-heterojunction tandem solar cells processed at low temperature.* Energy Environ Sci 9:81–88.
  - 18,1% efficiency – **heterojunction** c-Si subcell
  - Amorphous silicon layer requires **low temperature** processing of top perovskite subcell. ITO layer causes **parasitic light absorption**.

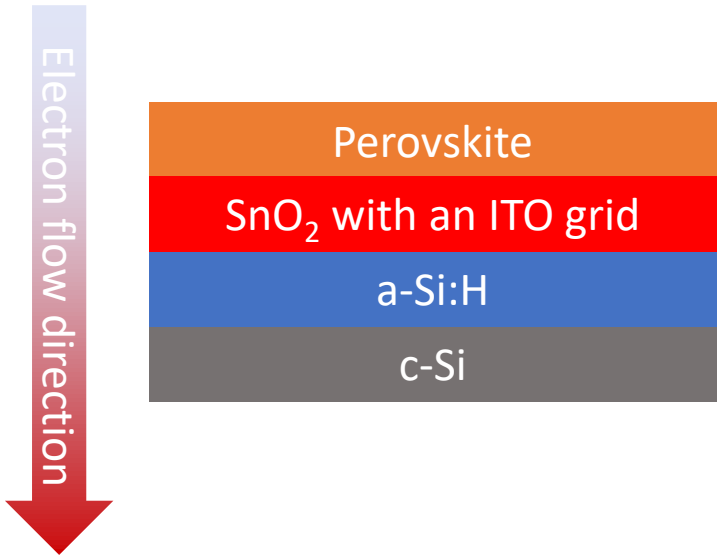

SnO_2 by ALD followed by ITO sputtering to form recombination layer

a-Si:H PECVD

1.1 Perovskite on silicon tandem solar cells

- Strategies for interconnecting the top and bottom subcells are varied
  - Werner (2016) *Efficient Monolithic Perovskite/Silicon Tandem Solar Cell with Cell Area >1 cm^2.* J Phys Chem Lett 7:161–166.
  - 19% efficiency – **heterojunction** c-Si subcell
  - Amorphous silicon layer requires low temperature processing of top perovskite subcell.
  - IZO layer causes **parasitic light absorption**.

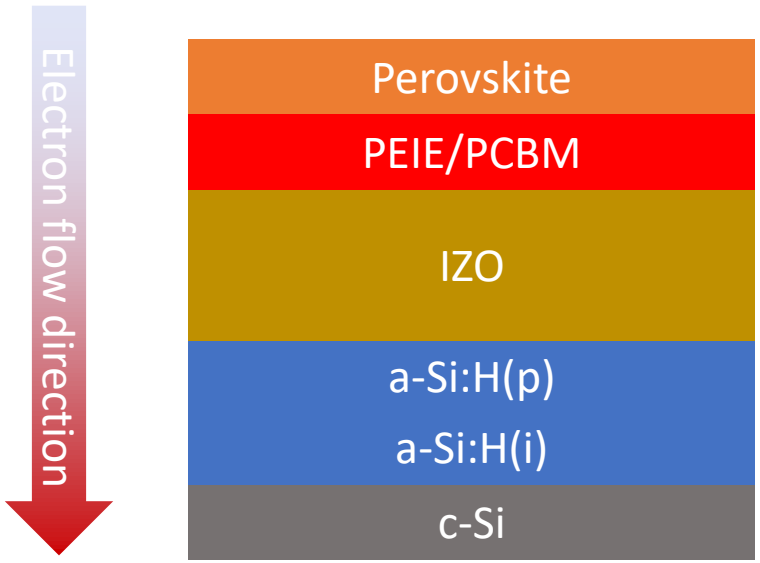

Sputtered IZO recombination layer

a-Si:H PECVD – first *intrinsic* then *p* doped is deposited

1.1 Perovskite on silicon tandem solar cells

- Strategies for interconnecting the top and bottom subcells are varied
  - Wu (2017) *Monolithic perovskite/silicon-homojunction tandem solar cell with over 22% efficiency.* Energy Environ Sci 10:2472–2479.
  - 22% efficiency, c-Si **homojunction**
  - Configuration **permits high temperature** processing on top of c-Si bottom subcell
  - ITO layer causes **parasitic light absorption** and metal grid reduces illumined area.

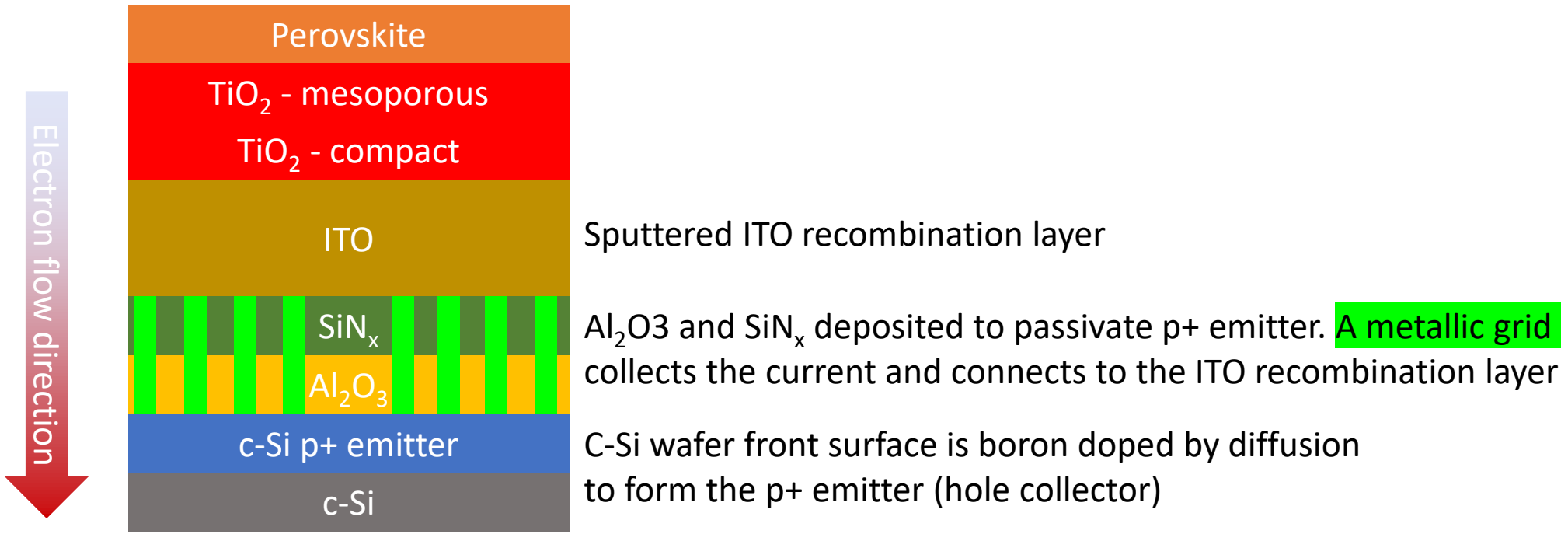

Sputtered ITO recombination layer

Al_2O3 and SiN_x deposited to passivate p+ emitter. A metallic grid collects the current and connects to the ITO recombination layer

C-Si wafer front surface is boron doped by diffusion to form the p+ emitter (hole collector)

1.1 Perovskite on silicon tandem solar cells

- Strategies for interconnecting the top and bottom subcells are varied
  - Bush (2017) *23.6%-Efficient Monolithic Perovskite/Silicon Tandem Solar Cells With Improved Stability.* Nat Energy 2:1–7.
  - 23.6% efficiency, c-Si **heterojunction**
  - Amorphous silicon layer requires low temperature processing of top perovskite subcell. ITO layer causes **parasitic light absorption**.

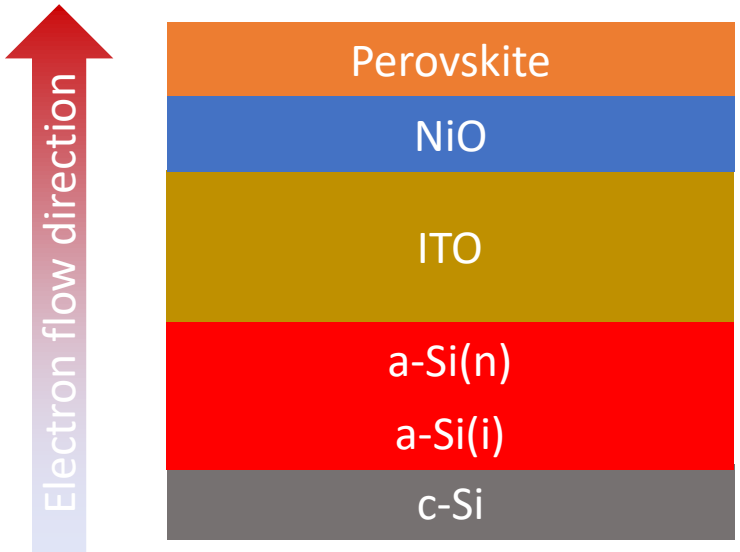

NiO is a p-type metal oxide which can deposited at low temperatures (>190 degC)

Sputtered ITO recombination layer

a-Si:H PECVD – first *intrinsic* then *n* doped is deposited

1.1 Perovskite on silicon tandem solar cells

- Strategies for interconnecting the top and bottom subcells are varied
  - Sahli (2018) *Improved Optics in Monolithic Perovskite/Silicon Tandem Solar Cells with a Nanocrystalline Silicon Recombination Junction.*
    Adv Energy Mater 8:1–8.
  - 25.2% efficiency, c-Si **heterojunction**
  - Amorphous silicon layer requires low temperature processing of top perovskite subcell.
  - **ITO Free – improved optics. Employs a tunnelling junction**

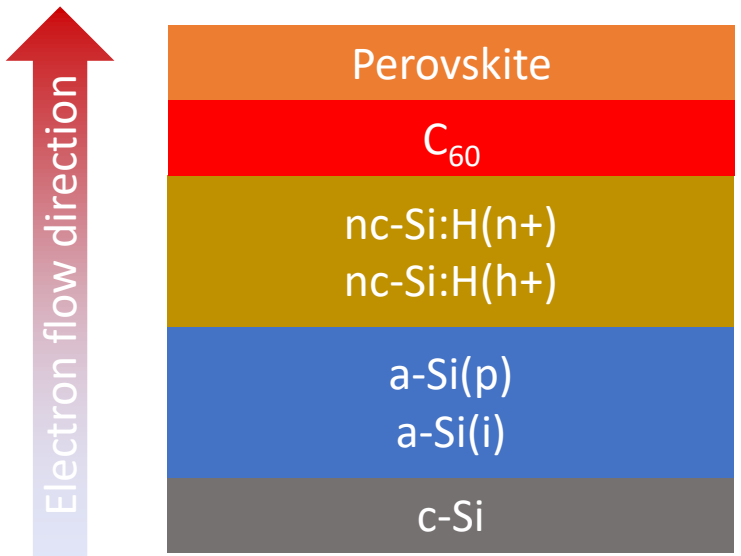

nc-Si n+/p+ tunnelling junction, deposited by PECVD <200 deg.C

a-Si hole selective contact for c-Si bottom cell

1.1 Perovskite on silicon tandem solar cells

- Strategies for interconnecting the top and bottom subcells are varied

  - Sahli (2018) *Fully textured monolithic perovskite/silicon tandem solar cells with 25.2% power conversion efficiency.* Nat Mater 17:820–826.

  - 25.2% efficiency, c-Si **heterojunction**

  - Amorphous silicon layer requires low temperature processing of top perovskite subcell.

  - ITO Free – improved optics. **Employs a tunnelling junction on a textured surface!**

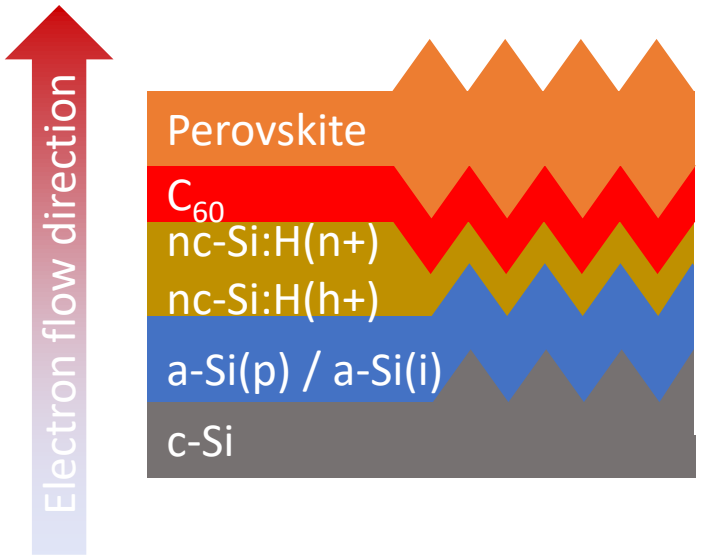

nc-Si n+/p+ tunnelling junction, deposited by PECVD <200 deg.C

1.1 Perovskite on silicon tandem solar cells

- Strategies for interconnecting the top and bottom subcells are varied
  - Zheng (2019) *Large-area 23%-efficient monolithic perovskite/homojunction-silicon tandem solar cell with enhanced uv stability using down-shifting material.*
    ACS Energy Lett 4:2623–2631.

    See also: Zheng (2018) Energy Environ Sci 11:2432–2443 & Zheng (2018) ACS Energy Lett 3:2299–2300.
  - 23% efficiency – **homojunction** c-Si subcell employing current state of the art PERC technology (passivate rear contact)
  - **16 cm² large area** (21.8%, Zheng (2018) ACS Energy Lett 3:2299–2300)
  - **FREE of a recombination or tunnel junction layer** – *perovskite electron selective contact is deposited directly onto silcon hole selective contact*
  - Compatible with **high temperature processing** for perovskite top subcell.

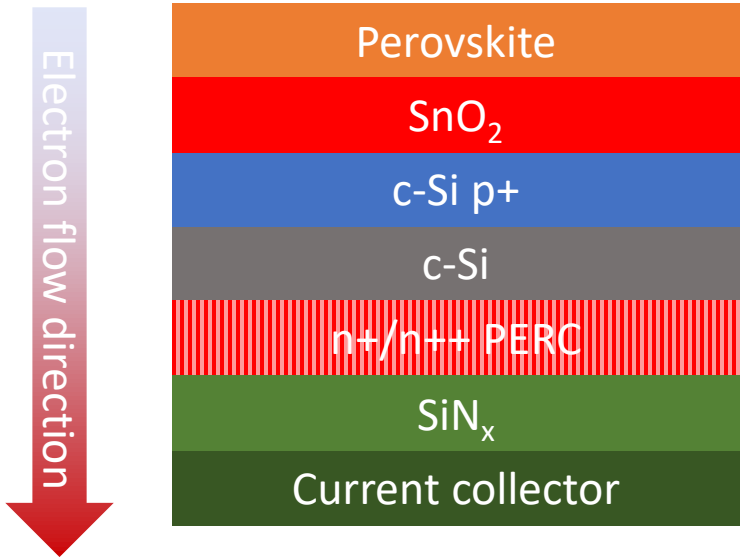

Thin 15nm solution processed SnO_2

Industry standard state of the art PERC c-Si bottom subcell

Passivated rear contact results in better collection of e-h generated from IR photons.

1.1 Perovskite on silicon tandem solar cells

- Strategies for interconnecting the top and bottom subcells are varied
  - Nogay (2019) *25.1%-Efficient monolithic perovskite/silicon tandem solar cell based on a p-type monocrystalline textured silicon wafer and high-temperature passivating contacts.* ACS Energy Lett 4:844–845.
  - 25.1% efficiency – c-Si subcell employing cost effective p-type wafers and thermally stable passivating contacts (800deg.C)
  - Compatible with **high temperature processing** for perovskite top subcell.

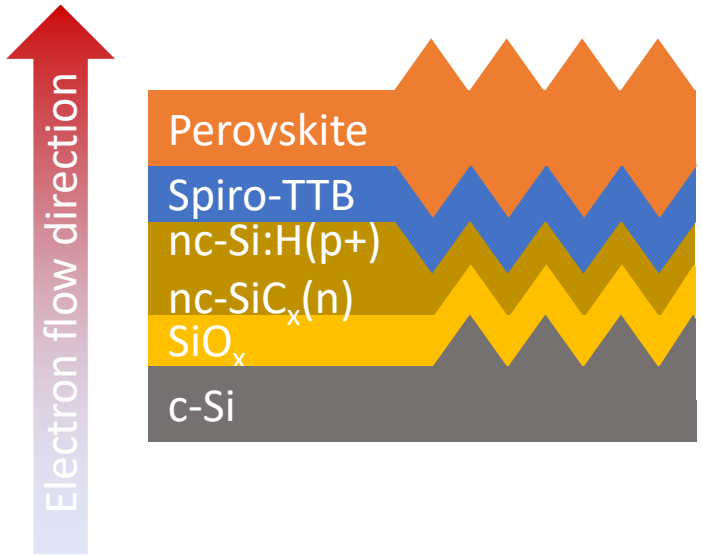

- SiCx by PECVD then heavily doped with phosphorous to form nc-SiCx(n).
- nc-Si(p+):H by PECVD to form the recombination junction

1.1 Perovskite on silicon tandem solar cells

- Strategies for interconnecting the top and bottom subcells are varied
  - Al-Ashouri (2020) *Monolithic perovskite/silicon tandem solar cell with >29% efficiency by enhanced hole extraction. Science (80-) 370:1300–1309.*
  - **RECORD 29.15% efficiency – Helmholtz Zentrum Berlin**
  - Still employs ITO recombination layer.
  - SiOx optical interlayer used to enhance IR transmittance to bottom cell and hence boost device performance.
  - New Self Assembled Monolayer developed as a hole selective contact for the Perovskite.

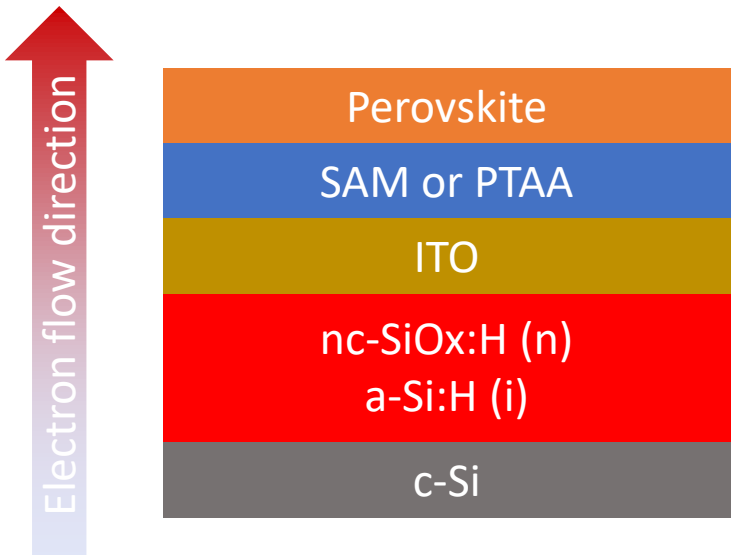

Self Assembled Monolayer – new hole selective contact

Layers deposited by PECVD

1.1 Perovskite on silicon tandem solar cells

- Take home messages are for recombination junction:
    - TCOs
        - parasitic light absorption
        - high lateral conductivity, shunting for large areas
    - Tunnelling diode
        - a-Si based limit top cell processing temperatures to below 200 deg.C
        - PECVD is slow, so can be problematic for upscaling.

- An excellent recent review:
  De Bastiani (2020) *Recombination junctions for efficient monolithic perovskite-based tandem solar cells: Physical principles, properties, processing and prospects.*
  Mater Horizons 7:2791–2809. https://doi.org/10.1039/d0mh00990c

Contents

1.2 Esaki Tunnelling Diode

- A tunnelling Esaki diode requires
  - highly (degenerately) doped layers
  - with abrupt changes in doping profiles
- Conduction and valence bands become energetically aligned
- Band bending is such that the physical distance between layers is sufficiently small to permit electrons and holes to tunnel and recombine.

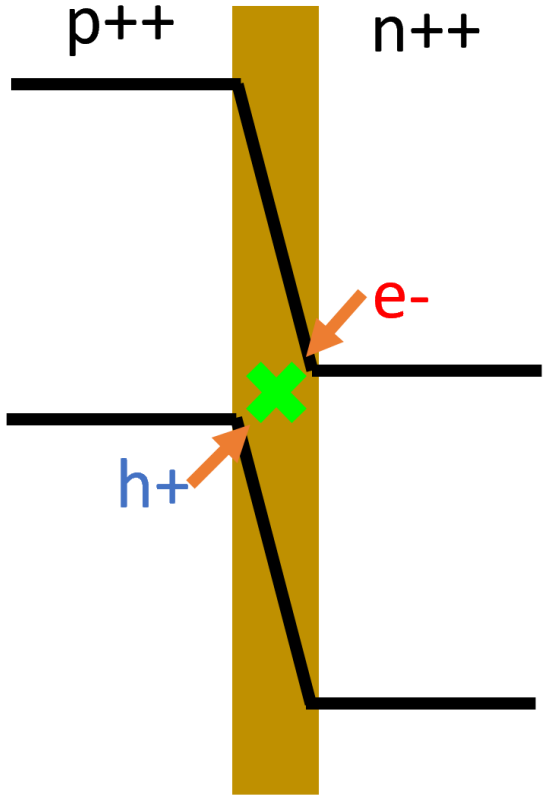

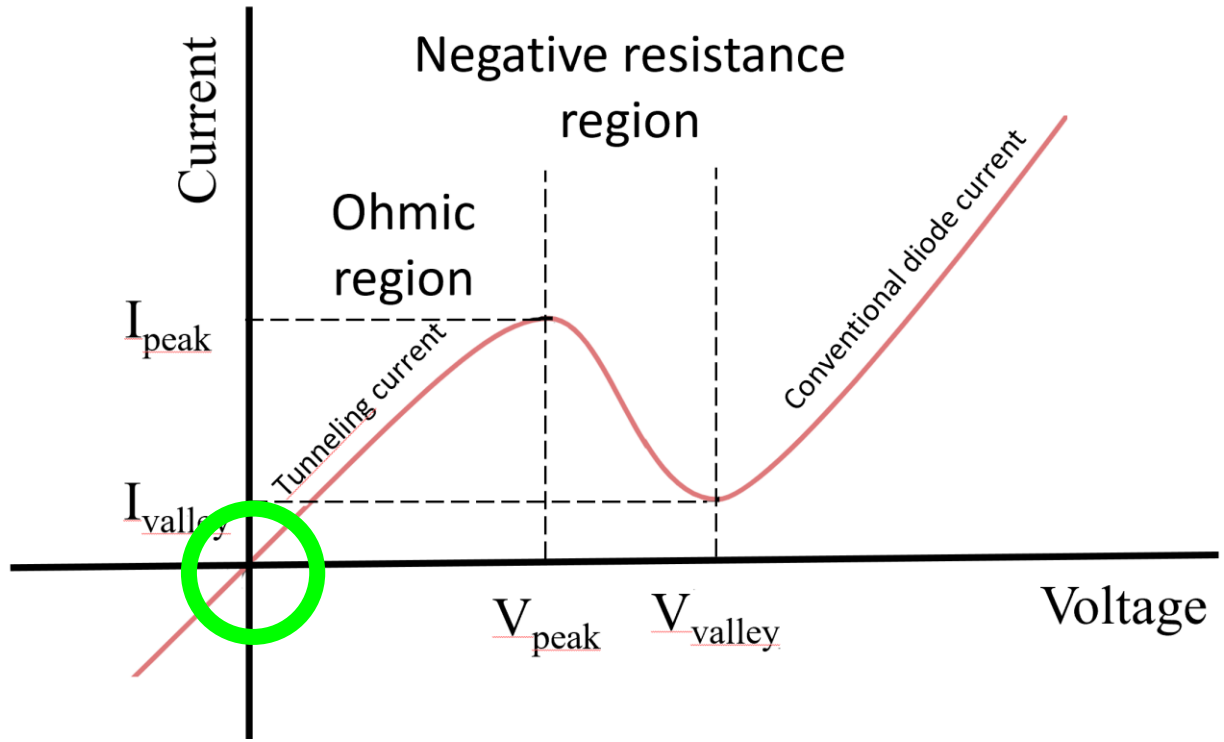

Contents

1.3 Gas Immersion Laser Doping (GILD)

- Gild Process
    1. Substrate is immersed in atmosphere containing dopant source
    2. Pulsed laser melts a thin surface layer
    3. Dopant adsorbed at sample surface dissolves into melt and rapidly diffuses within melt region
    4. Melt recrystallizes
    5. Dopant adsorption
    6. Laser fires further along

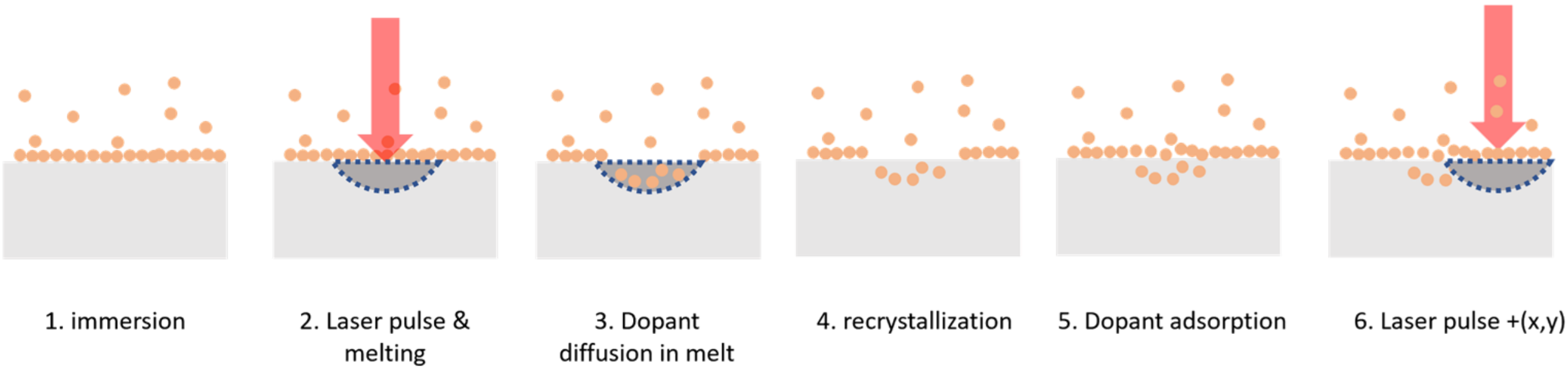

1.3 Gas Immersion Laser Doping (GILD)

- Doping profile control

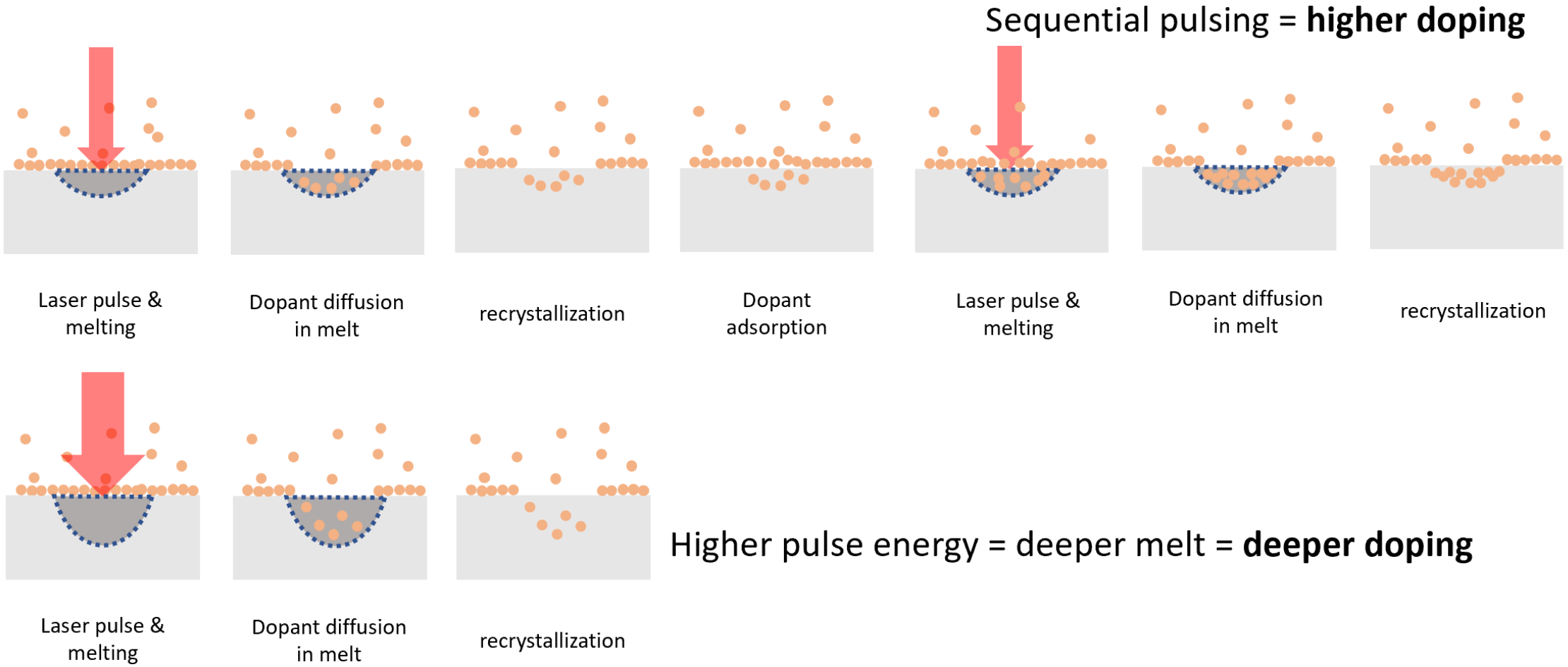

1.3 Gas Immersion Laser Doping (GILD)

- Tunnel junctions should be possible because:
  - High dopant incorporation (above solubility limit)
  - Molten zone and short time scales (ns) results in abrupt dopant concentrations

- Examples of reports of highly doped silicon by GILD
  - Carey (1989) *In-situ doping of silicon using the gas immersion laser doping (GILD) process.* Appl Surf Sci 43:325–332.
  - Kerrien (2002) *Ultra-shallow, super-doped and box-like junctions realized by laser-induced doping.* Appl Surf Sci 186:45–51.

Contents

2 Phosphorus GILD on c-Si wafers)

- **<u>Goal</u>: Phosphorous Gas Immersion Laser Doping of p+ silicon emitters**
  - to form n++/p+ tunnelling interface
  - on large surface areas – hence scalable

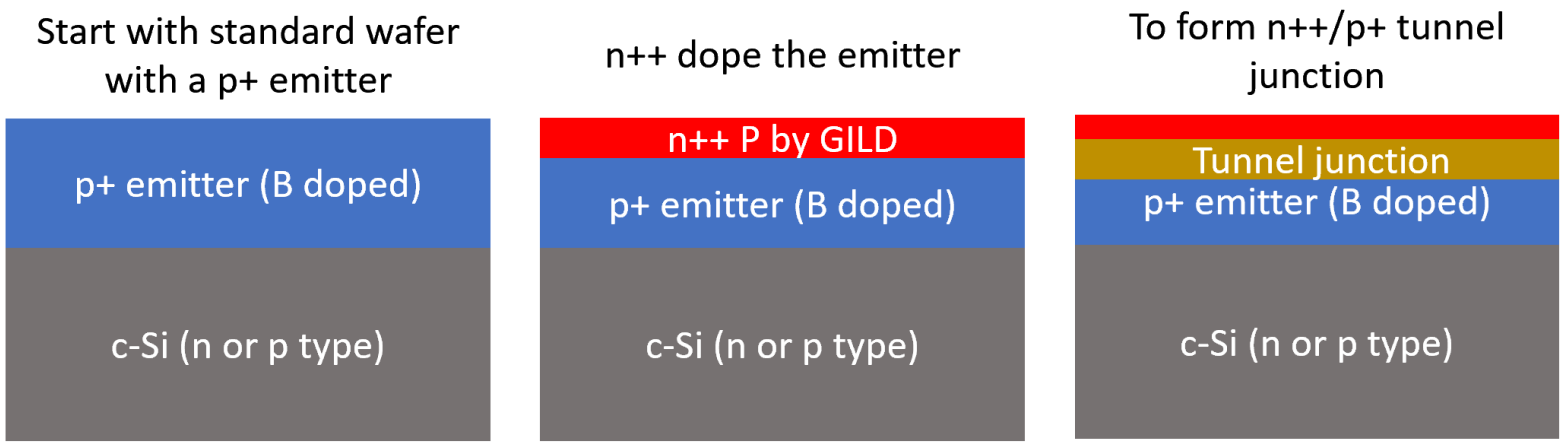

- Similar approach taken by:
  - Bellanger (2018) *Silicon Tunnel Junctions Produced by Ion Implantation and Diffusion Processes for Tandem Solar Cells.* IEEE J Photovoltaics 8:1436–1442.
  - Fave (2017) *Fabrication of Si tunnel diodes for c-Si based tandem solar cells using proximity rapid thermal diffusion.* Energy Procedia 124:577–583.

  - Was successful, but employed **Ion implantation or sacrificial wafers**…

2 Phosphorus GILD on c-Si wafers)

- **Apparatus setup and approach**
  - Start with c-Si wafer with boron doped emitter
  - Dope emitter with Phosphorus using GILD

  - Dopant source is $POCl_3$
    - Industry standard P source
    - Safe (unlike Phosphine PH_3)
    - Cost effective

- 1064nm ns pulsed laser coupled to highspeed x-y galvano mirror head

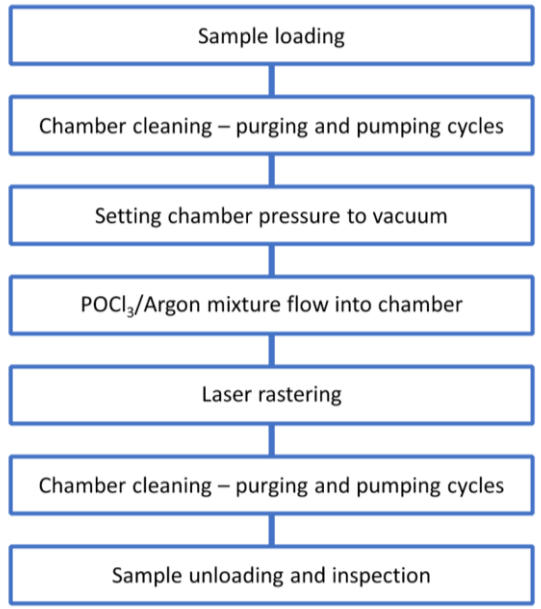

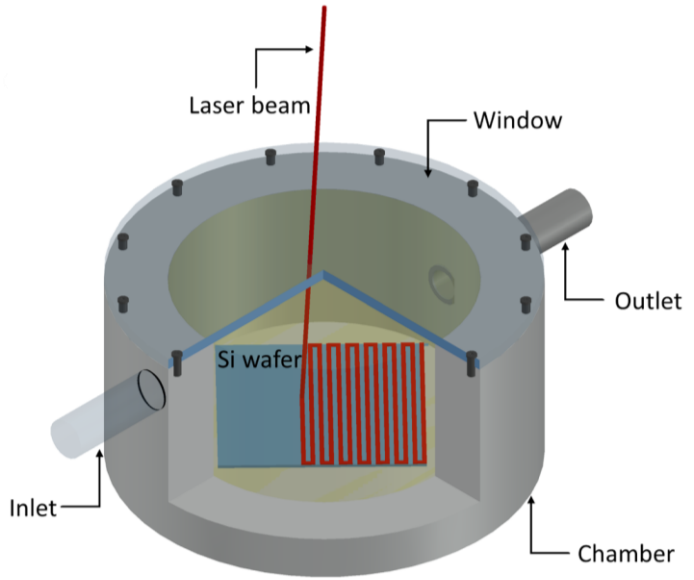

Contents

2.1 Overview of our past work

- **Approach**
  - GILD on p type c-Si wafer (low doping)

- Work presented at:

Gaspar (2020) *Laser Phosphorous Doping at High Scan Rates for Crystalline Junction Formation in Silicon/Perovskite Tandem Solar Cells.* The 30th International Photovoltaic Conference Science and Engineering Conference (PVSEC-30) & Global Photovoltaic Conference (GPVC 2020). Jeju, Republic of Korea

Gaspar (2020) *Sequential silicon surface melting and atmospheric pressure phosphorus doping for crystalline tunnel junction formation in silicon/perovskite tandem solar cells*.
In: 37th EU PVSEC 2020, European PV Solar Energy Conference and Exhibition, Lisbon, Portugal

Contents

2.1 Overview of our past work

Scanning Electron Microscopy (SEM)

	d = 2 µm	d = 3.5 µm	d = 4 µm
n = 1x	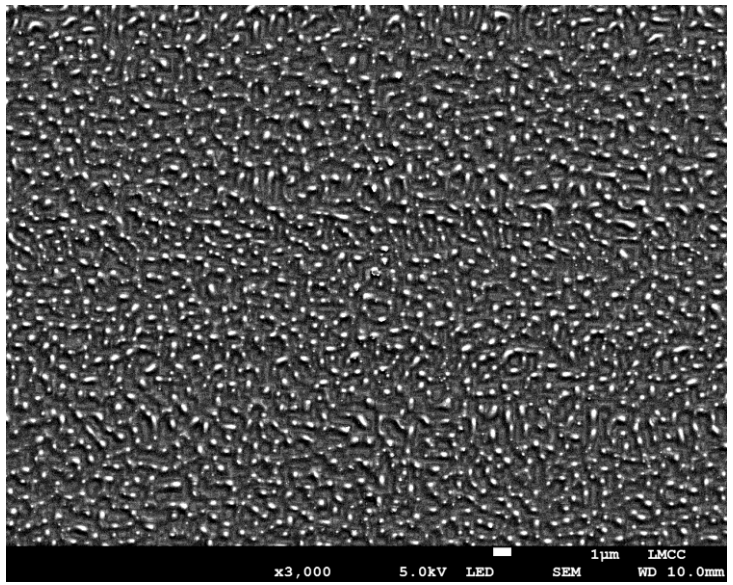	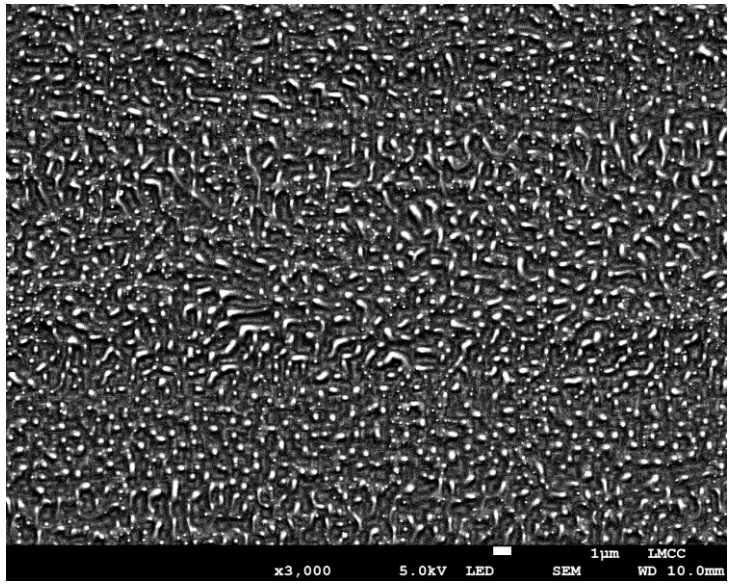	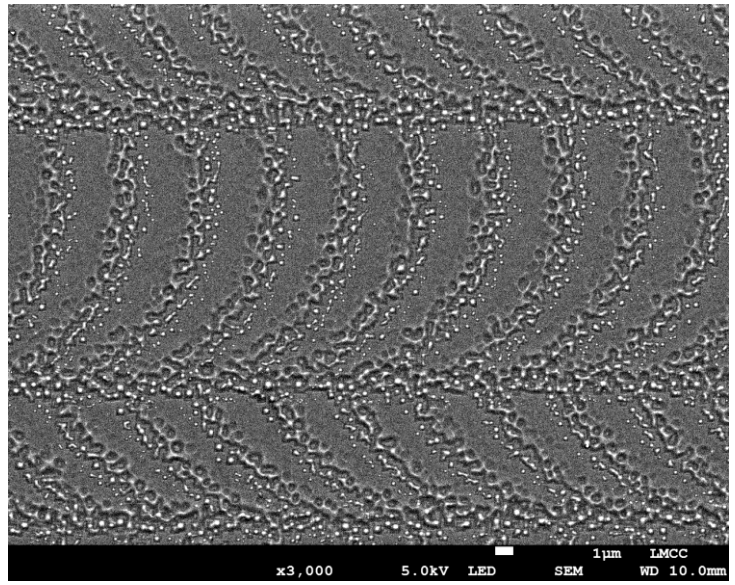
n = 2x	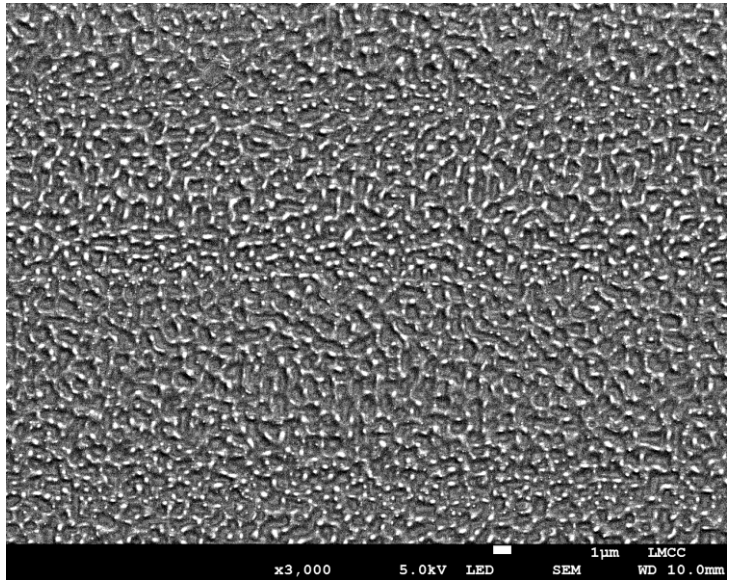		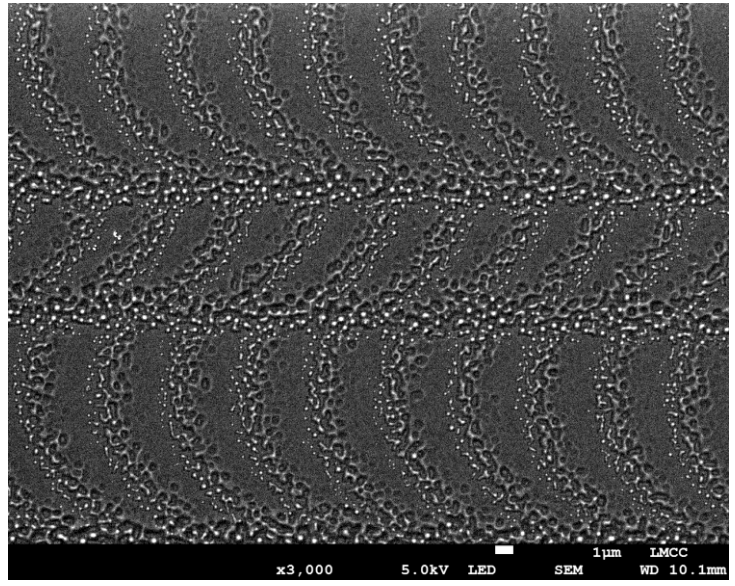

2.1 Overview of our past work

Scanning Electron Microscopy (SEM)

d = 2 µm

d = 3.5 µm

d = 4 µm

n = 1x

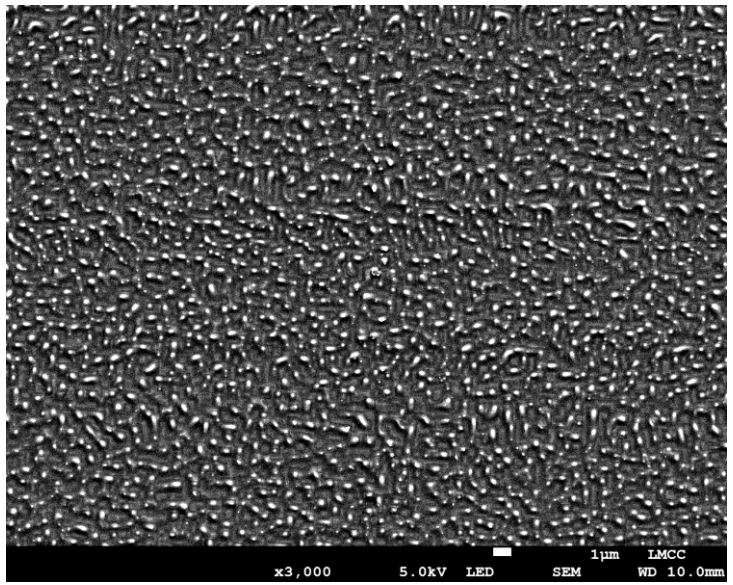

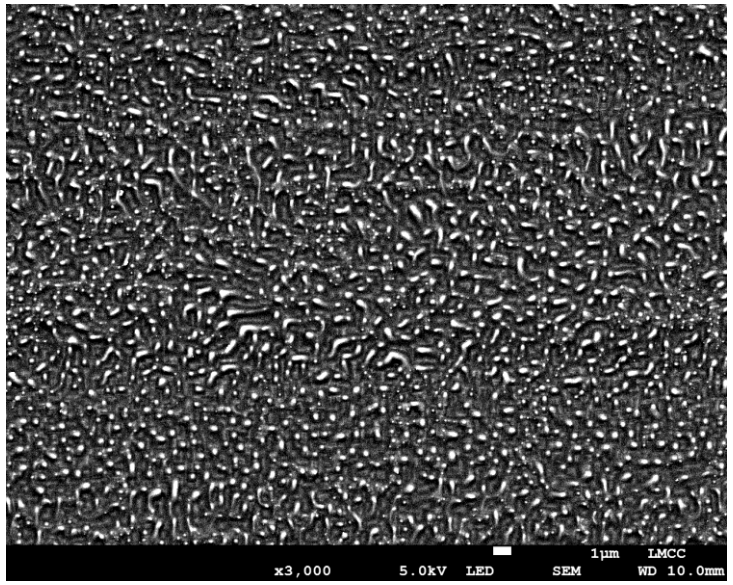

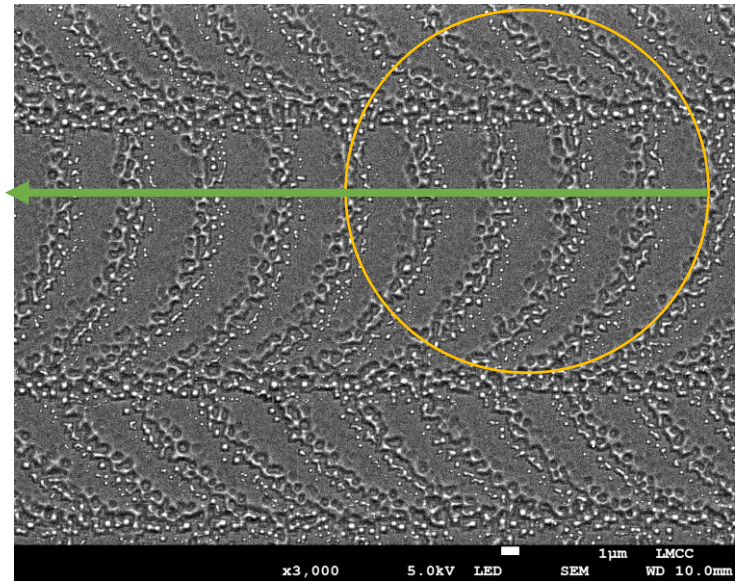

n = 2x

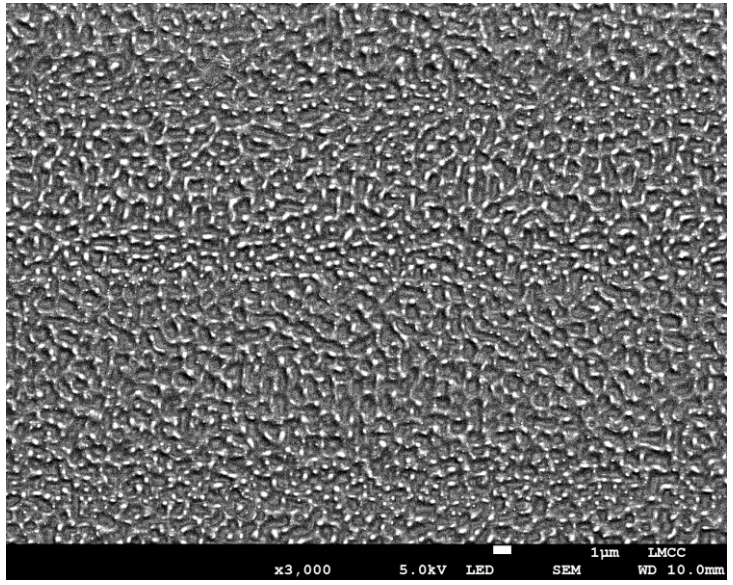

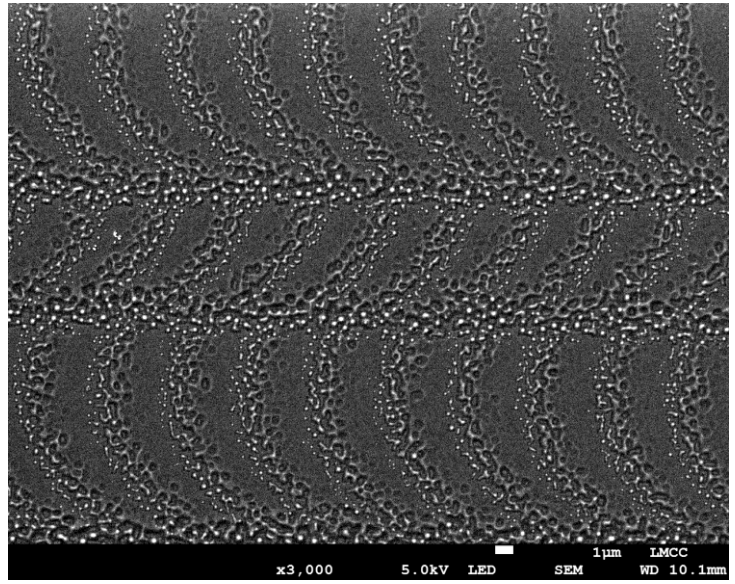

2.1 Overview of our past work

Scanning Electron Microscopy (SEM)

d = 2 µm

d = 3.5 µm

D = 10 µm

n = 1x

n = 2x

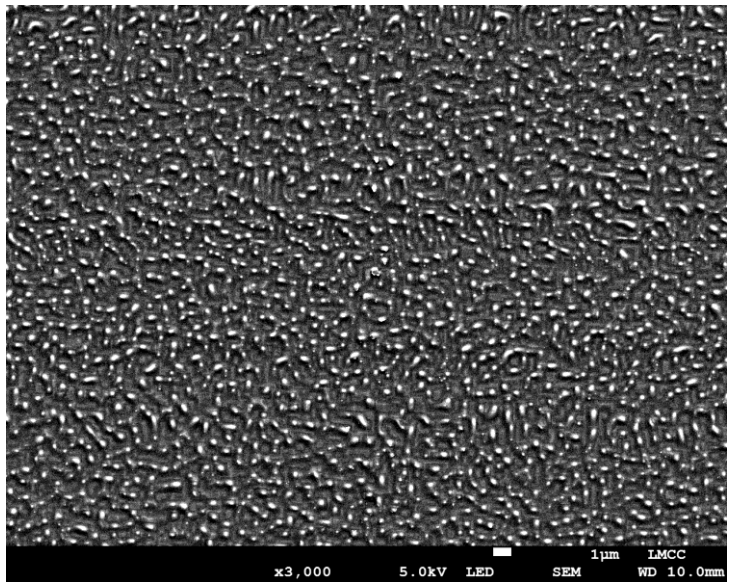

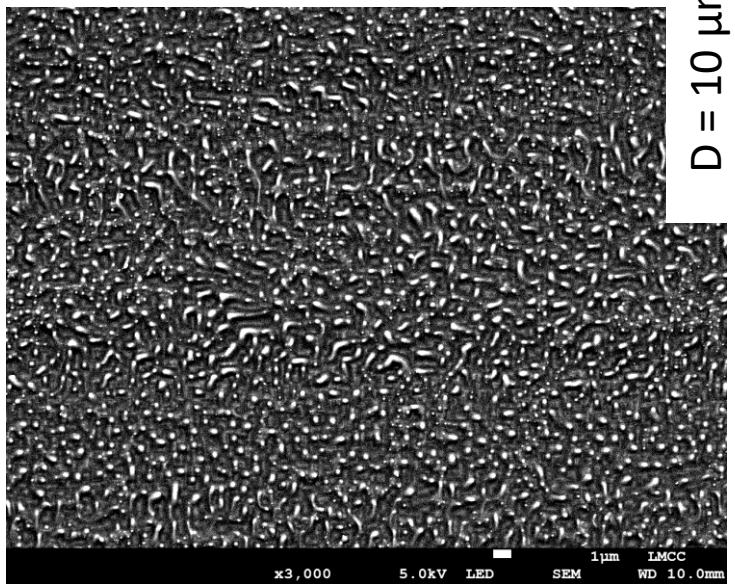

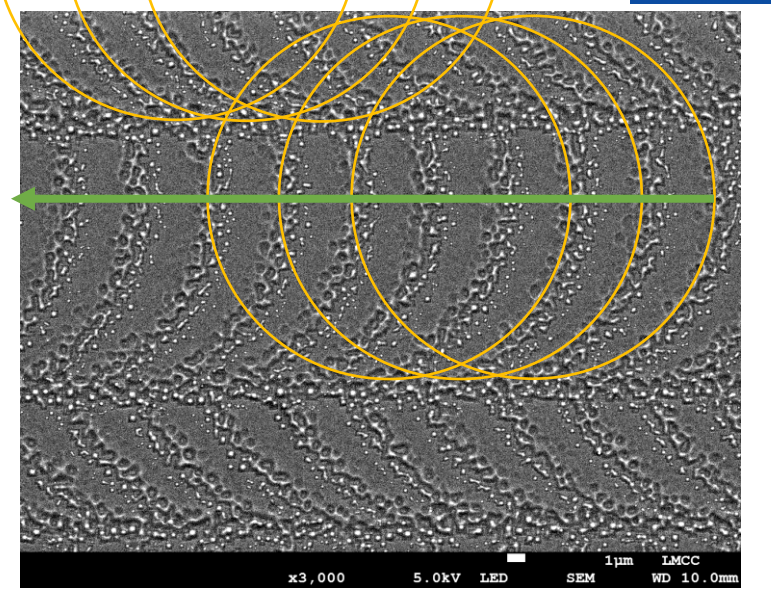

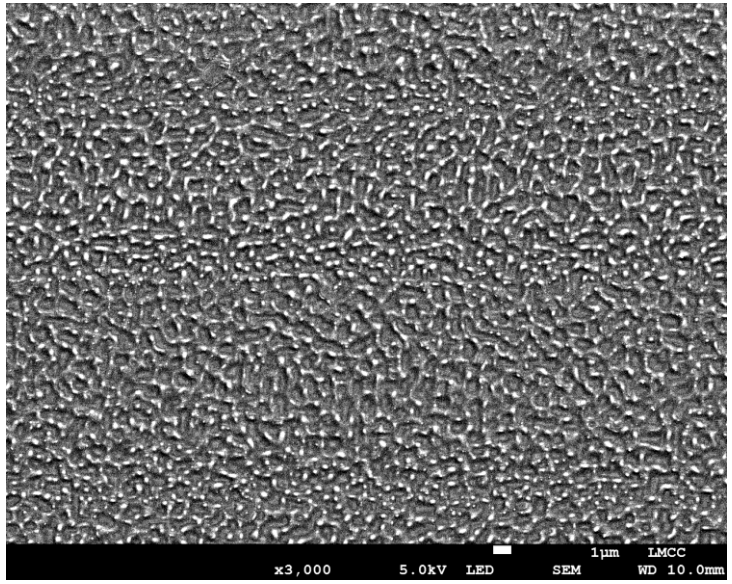

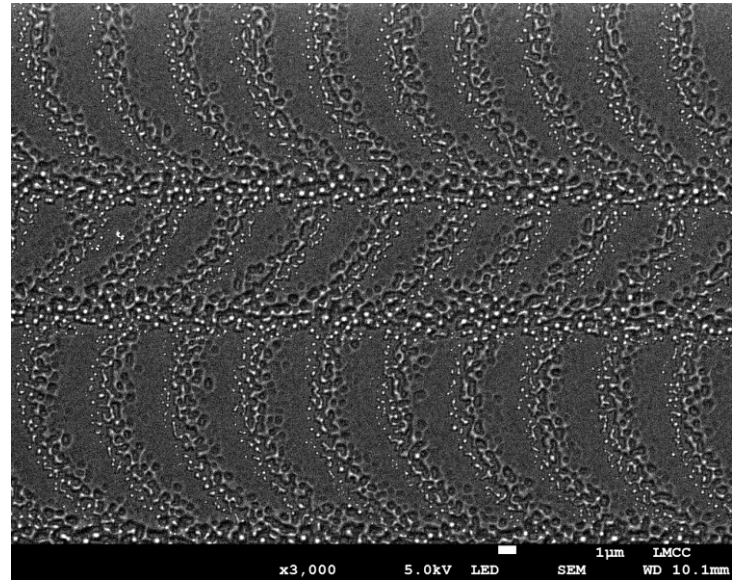

Secondary Ion Mass Spectrometry (SIMS)

Varied number of passes (n)
d = 2 µm

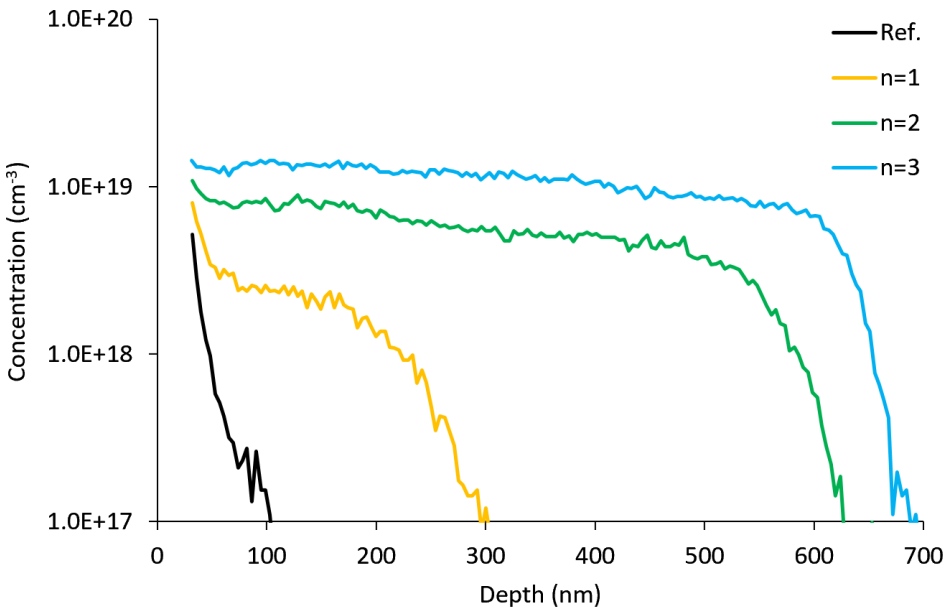

Comparison laser spot spacing: d = 1 µm vs d = 2 µm
Varied number of passes (n)

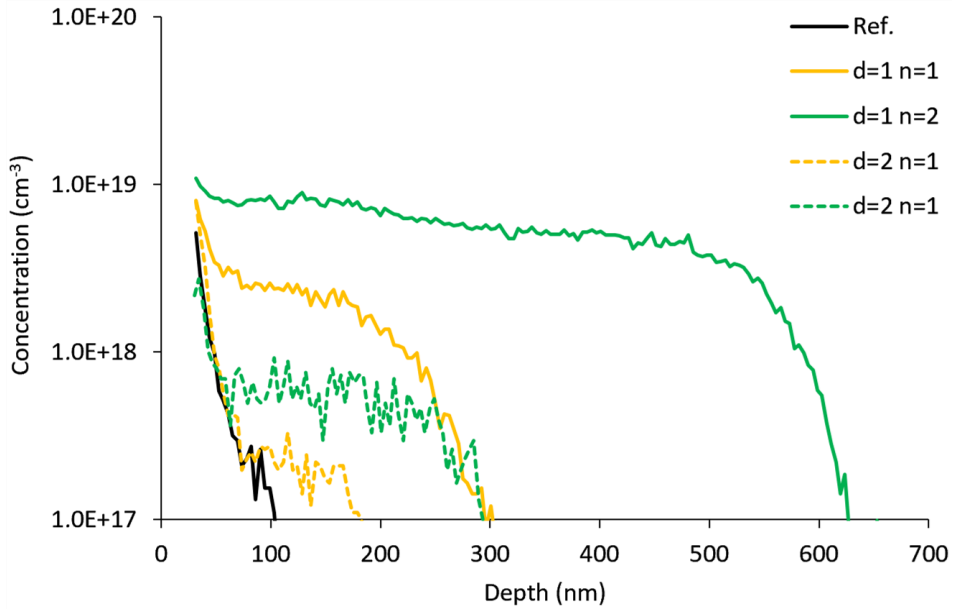

Laser pulse energy	E_P = 40 µJ
Laser line spacing	D = 10 µm

Contents

Scanning Electron Microscopy (SEM)

p vs p++/p+ wafers

d = 2 µm; n = 1x

p wafer

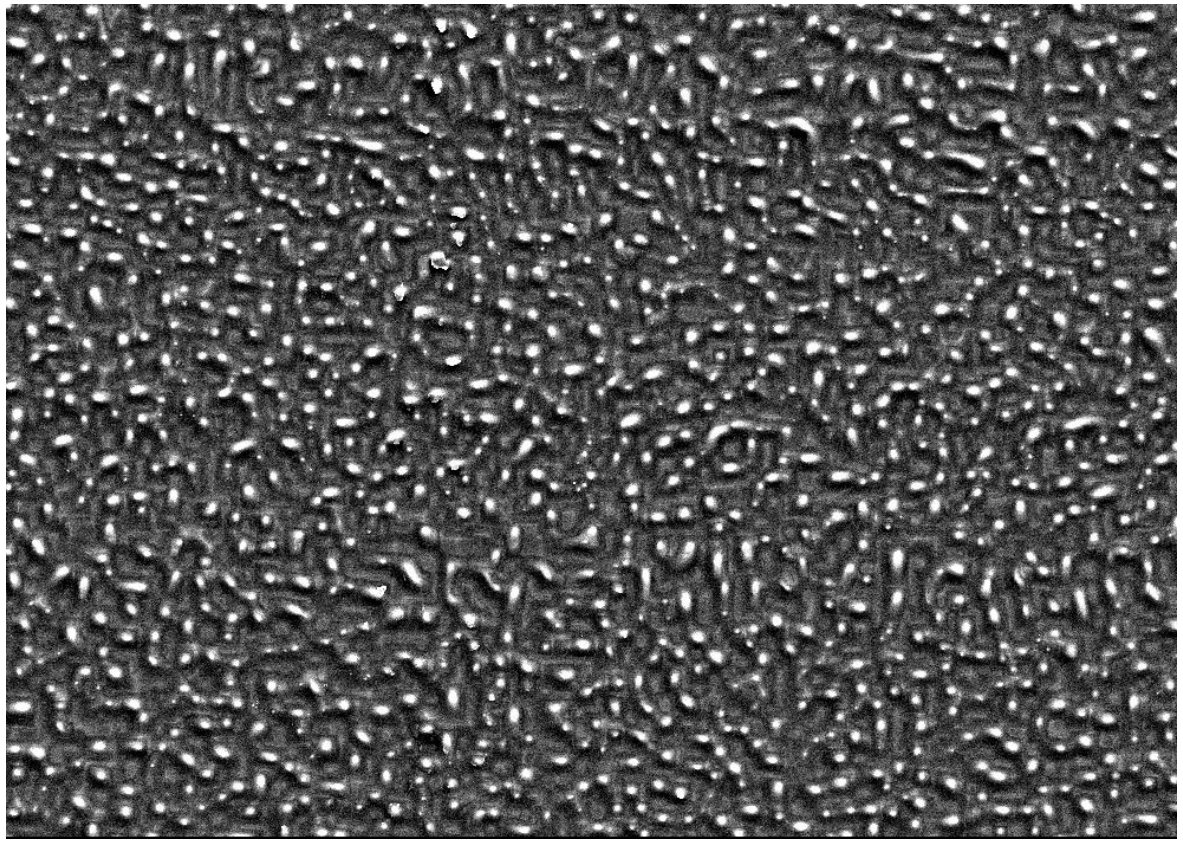

p++/p+ wafer

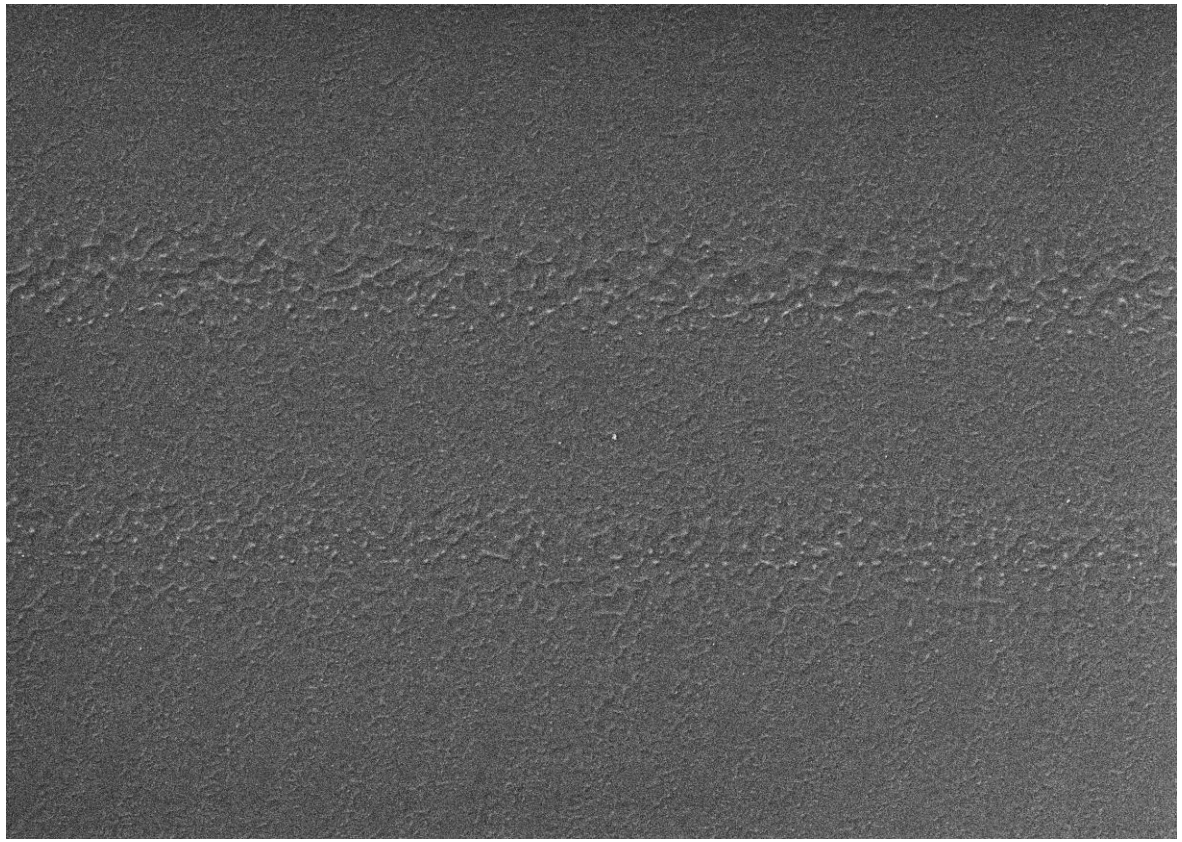

Magnification 4000x

Scanning Electron Microscopy (SEM)

p vs p++/p+ wafers

d = 2 µm; n = 1x

p wafer

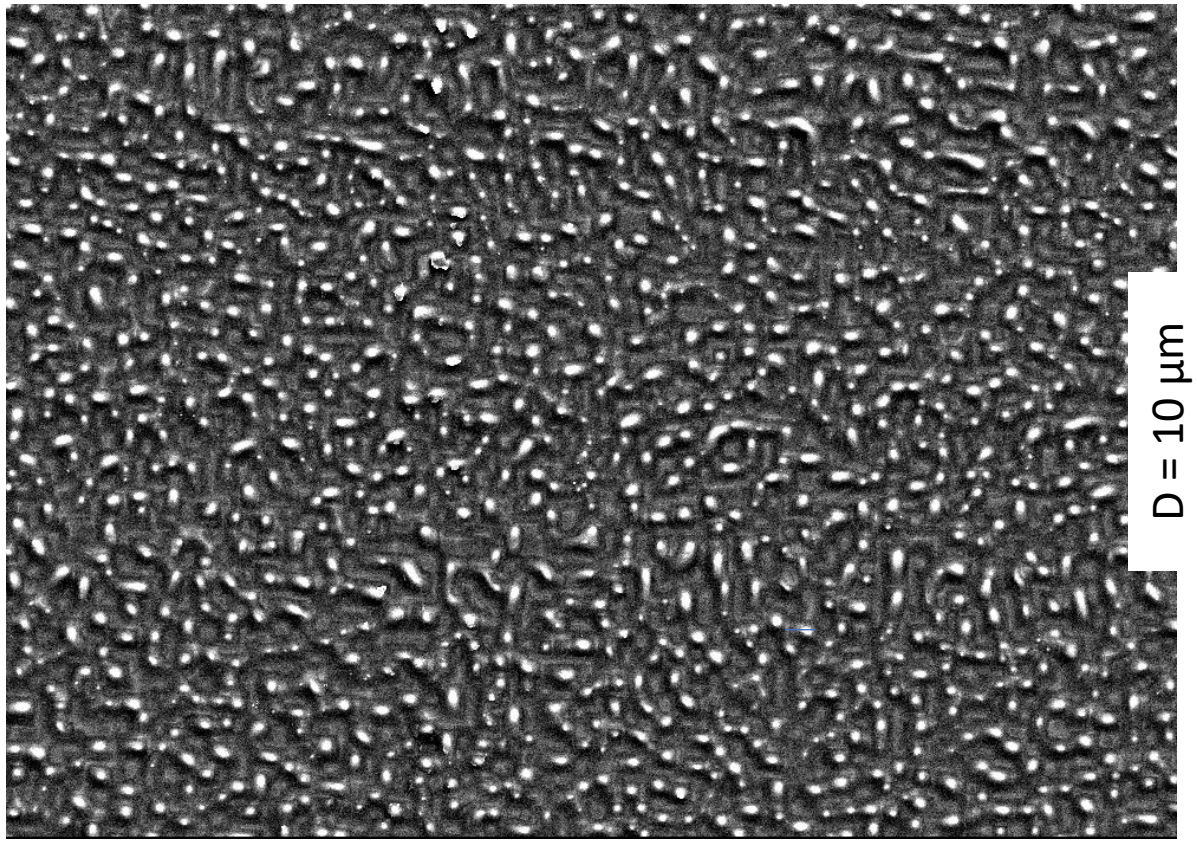

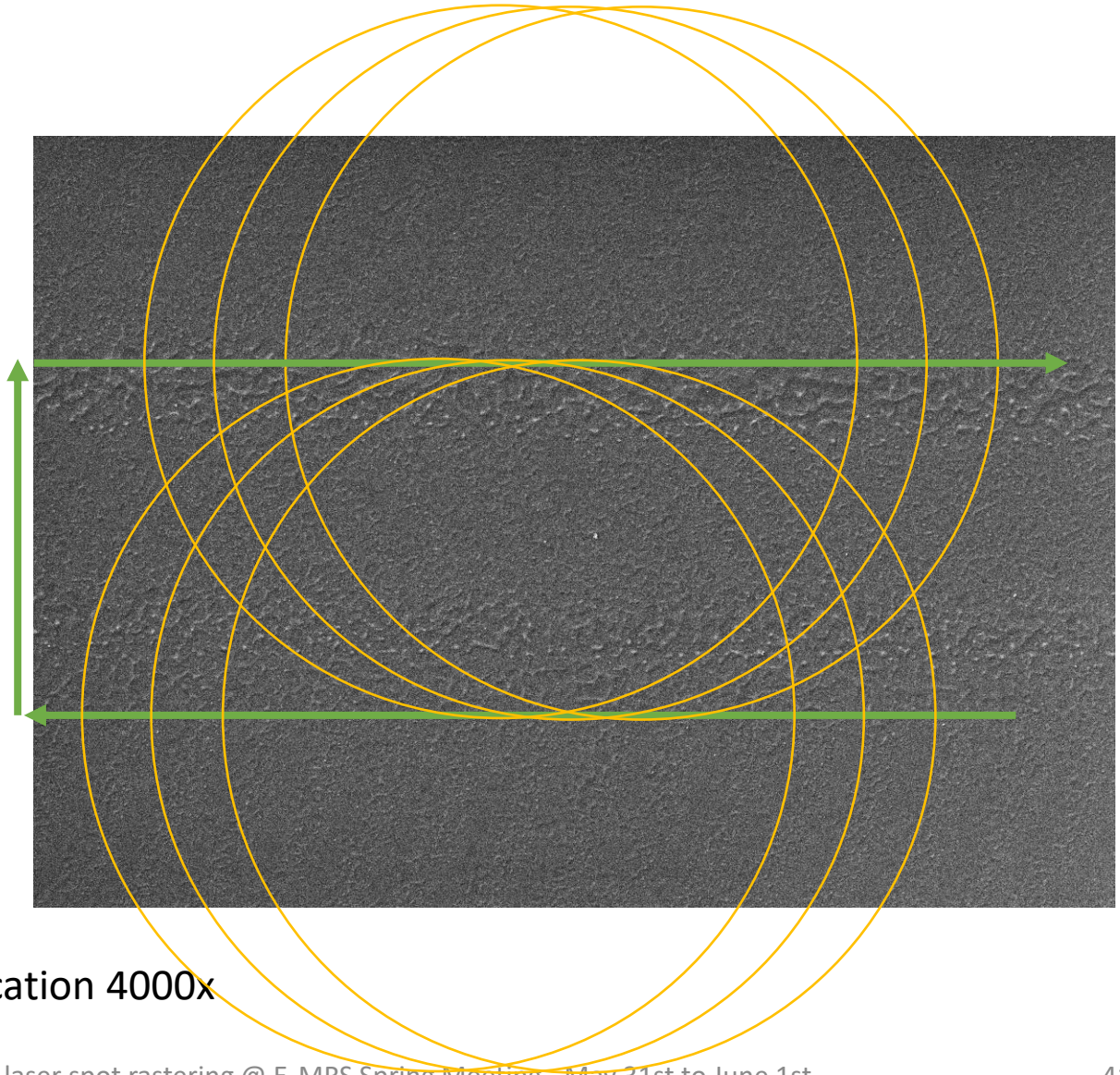

Magnification 4000x

2.2 Current results

Scanning Electron Microscopy (SEM)

d = 1 µm | d = 2 µm | d = 3 µm

n = 1x

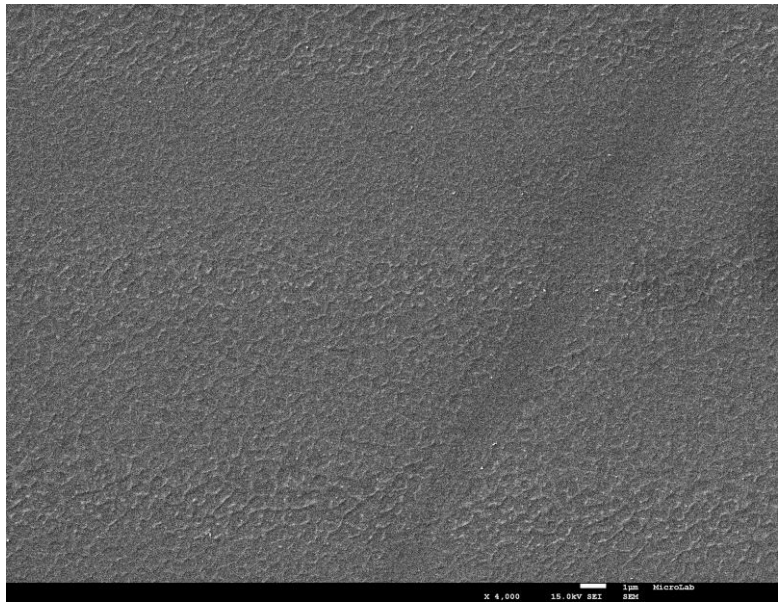

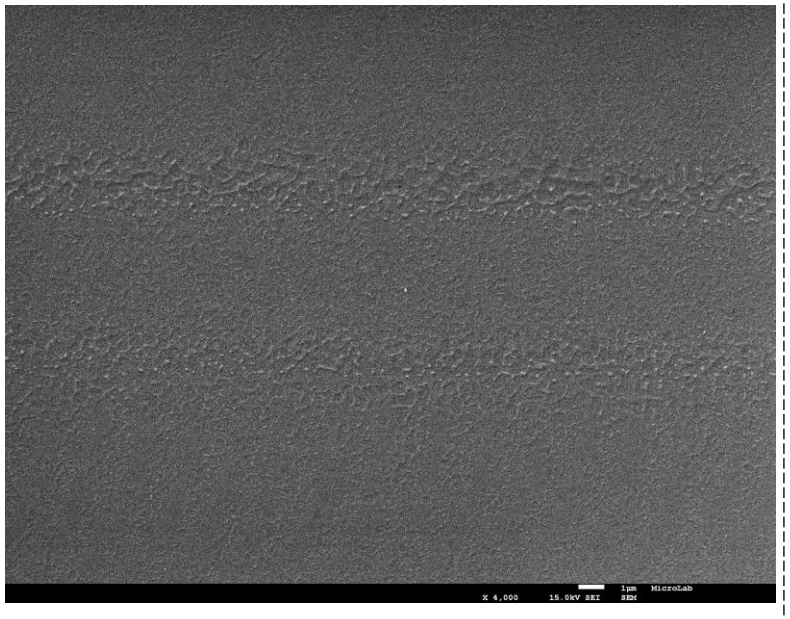

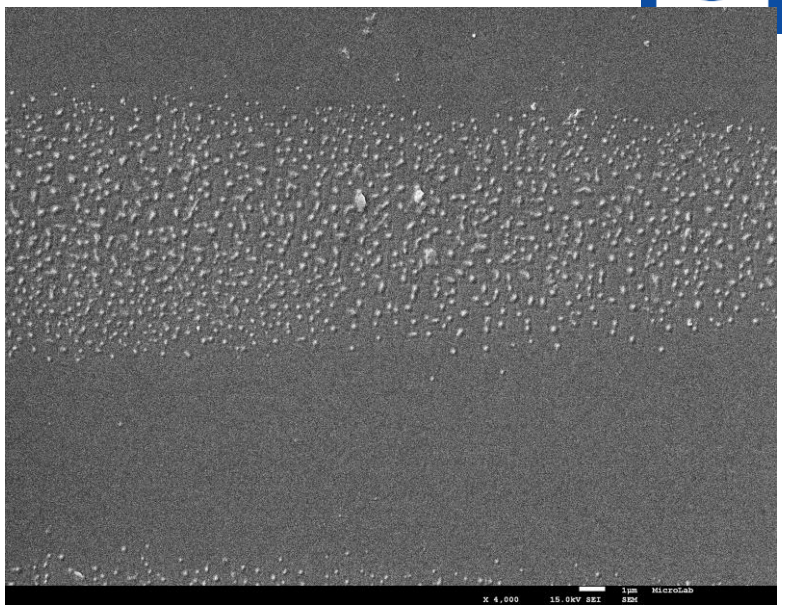

n = 3x

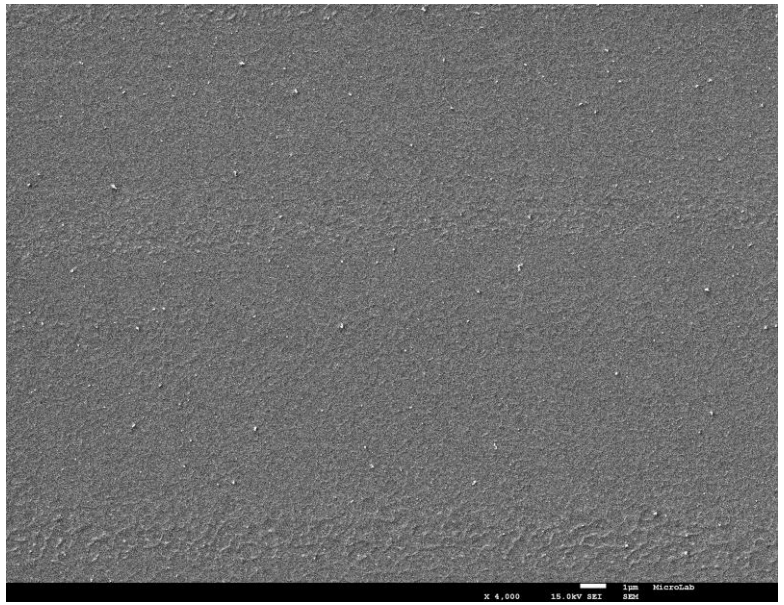

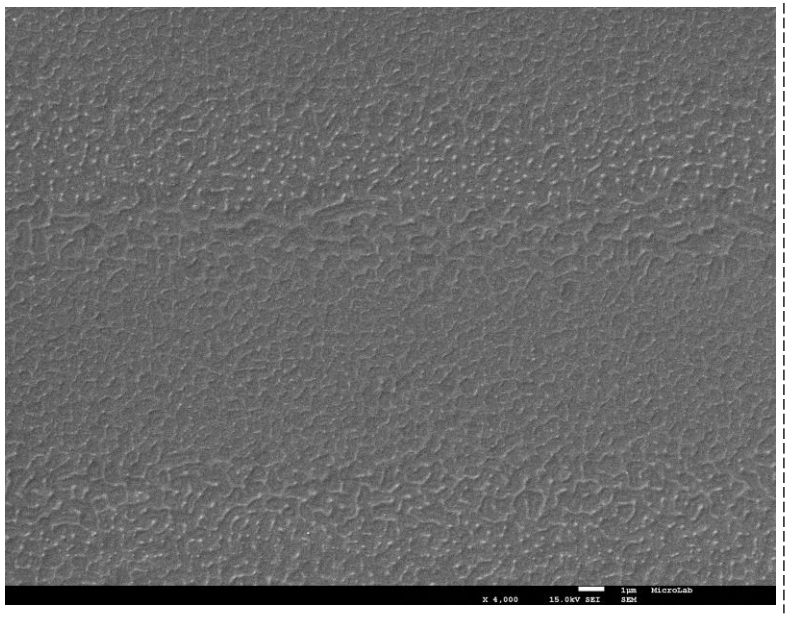

Magnification 4000x

Atomic Force Microscopy (AFM)

Processing parameters: d = 2 µm; n = 1x

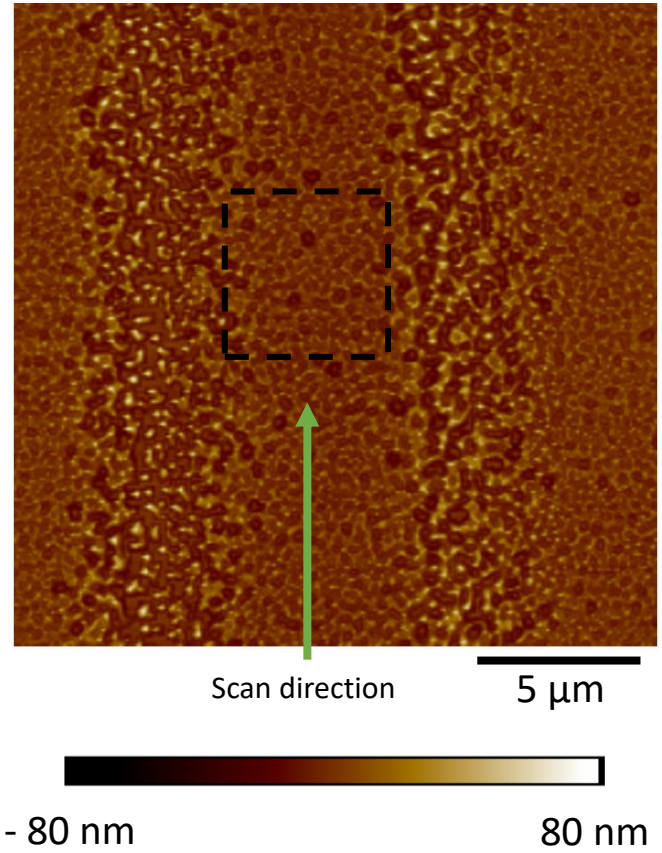

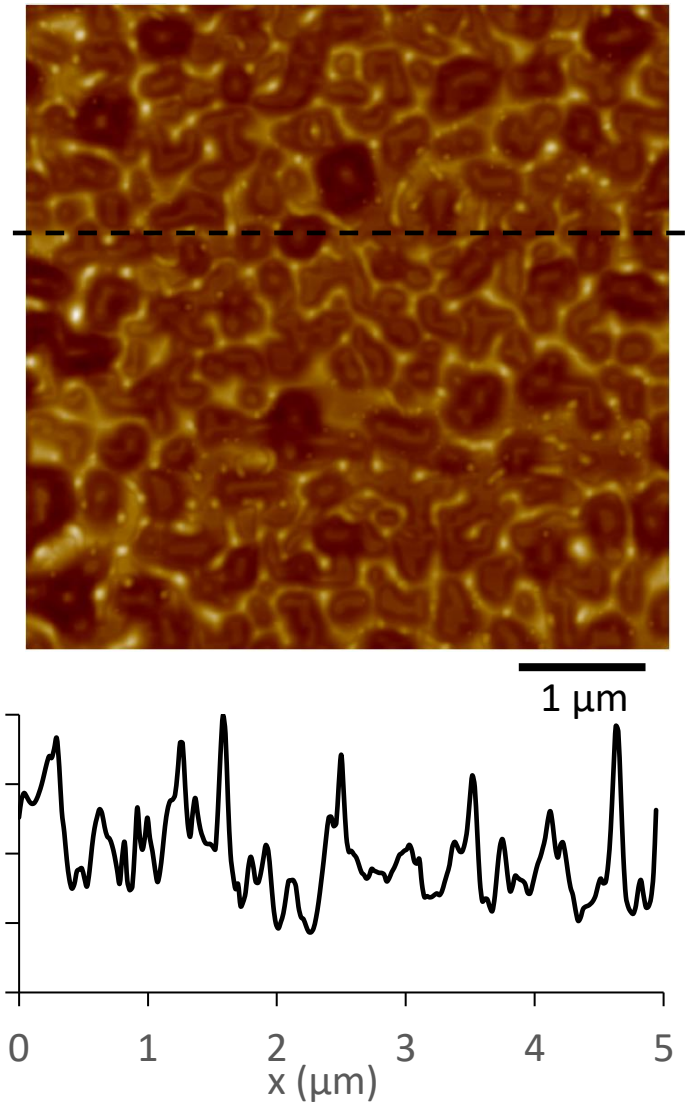

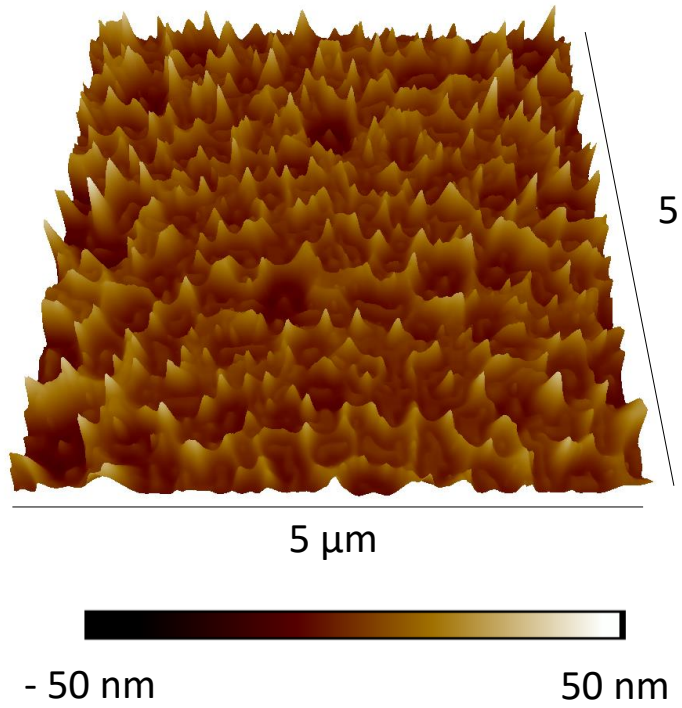

2.2 Current results

Atomic Force Microscopy (AFM)

d = 1 µm; n = 1x

RMS = 4.7 nm

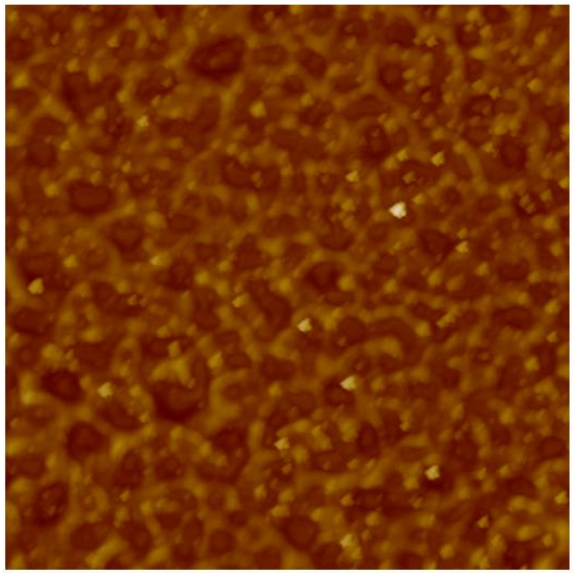

1 µm

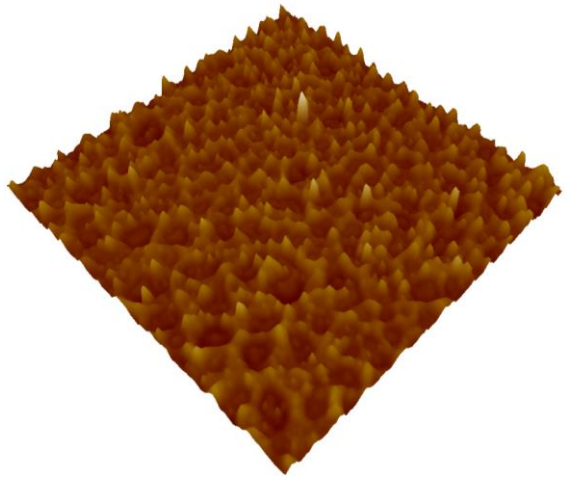

d = 2 µm; n = 1x

RMS = 7.1 nm

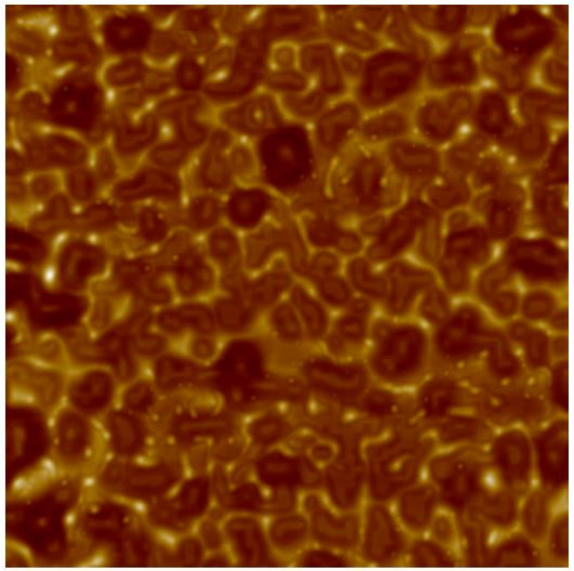

1 µm

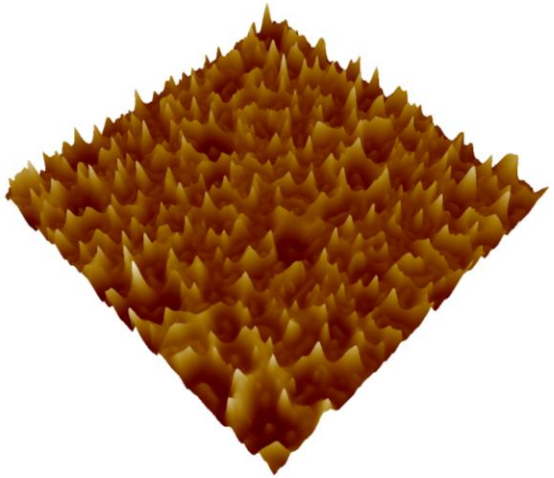

d = 3 µm; n = 1x

No clear interaction was verified!

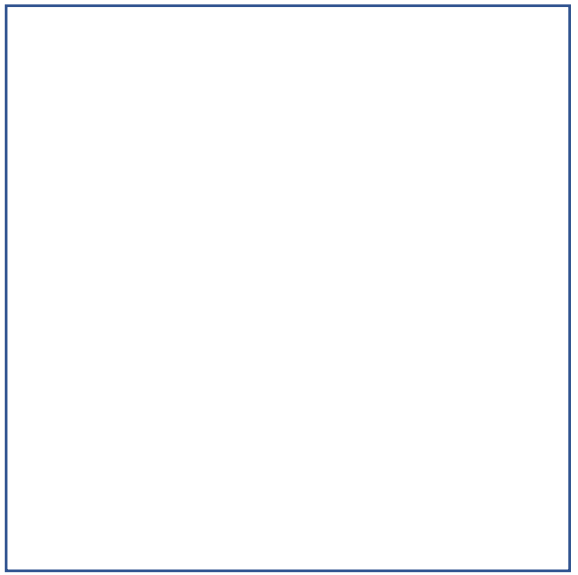

Unprocessed samples with no significant roughness!

RMS = 0.5 nm

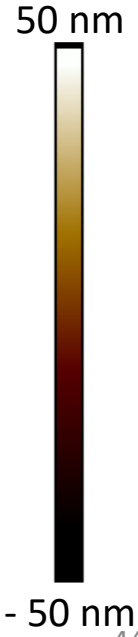

2.2 Current results

Atomic Force Microscopy (AFM)

d = 1 µm; n = 1x

RMS = 4.7 nm

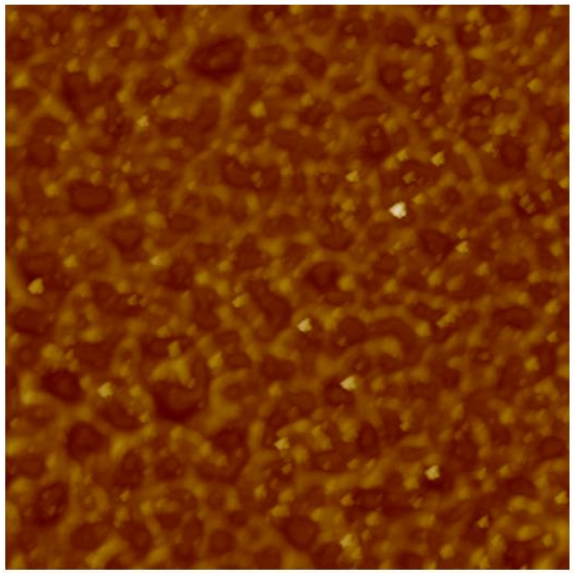

1 µm

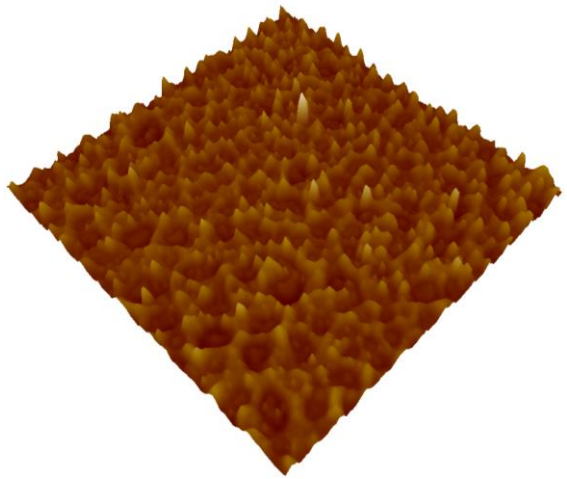

d = 2 µm; n = 1x

RMS = 7.1 nm

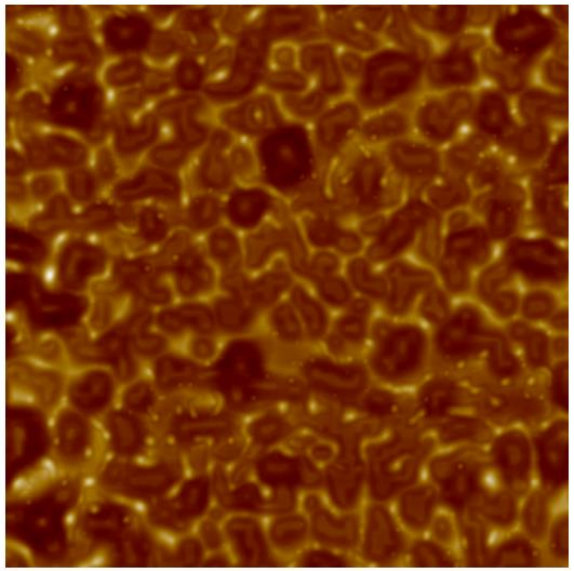

1 µm

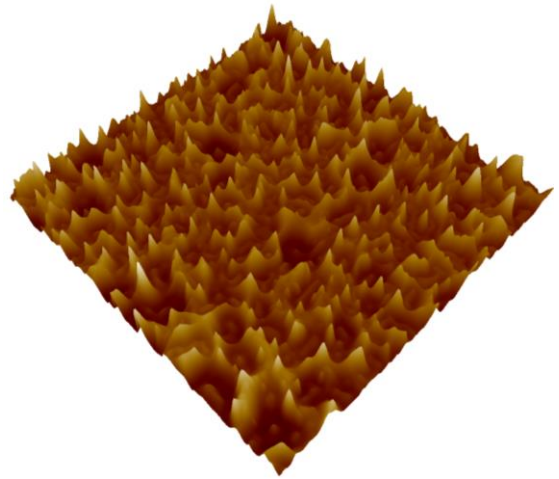

d = 3 µm; n = 3x

Unless rastered with a larger number of scans

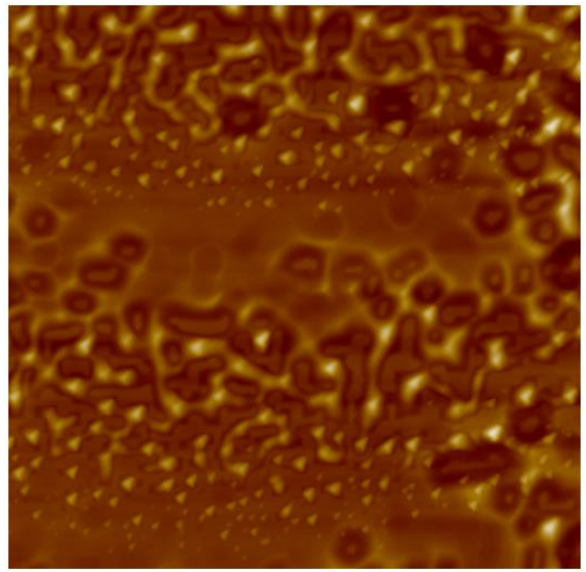

1 µm

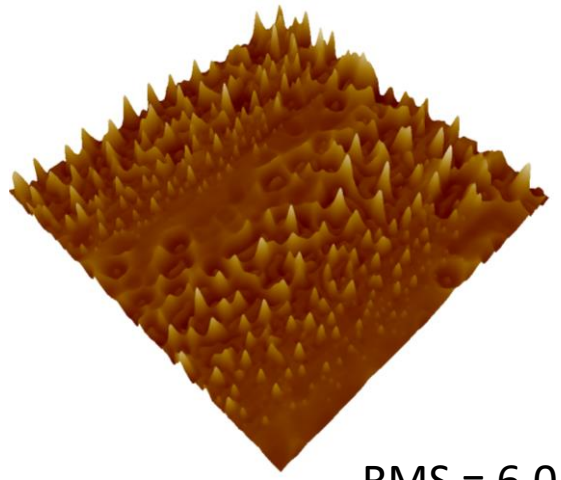

RMS = 6.0 nm

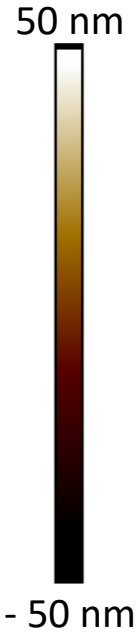

2.2 Current results

Atomic Force Microscopy (AFM)

d = 1 µm; n = 1x

RMS = 4.7 nm

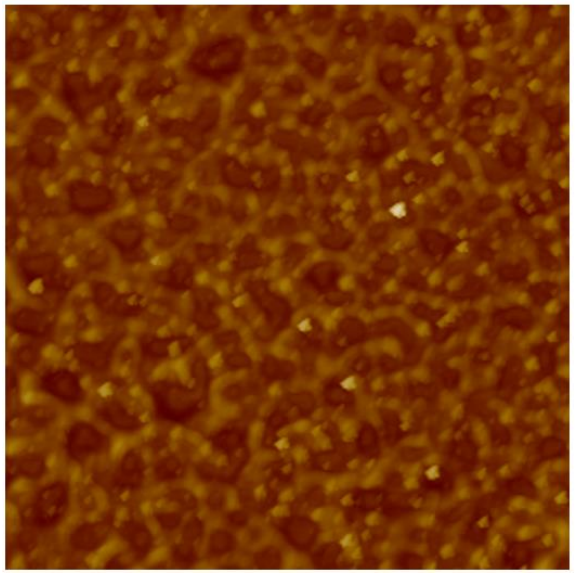

1 µm

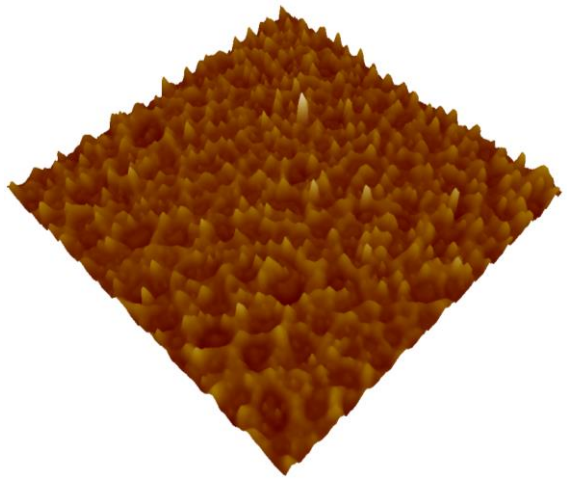

And if increasing the number of scans

d = 1 µm; n = 9x

RMS = 6.8 nm

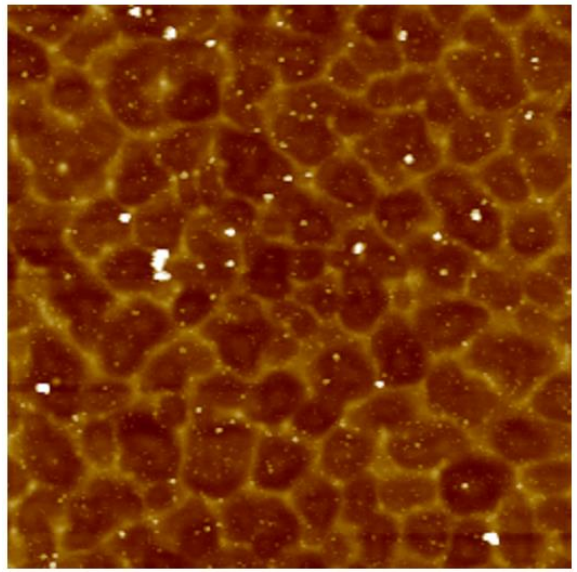

1 µm

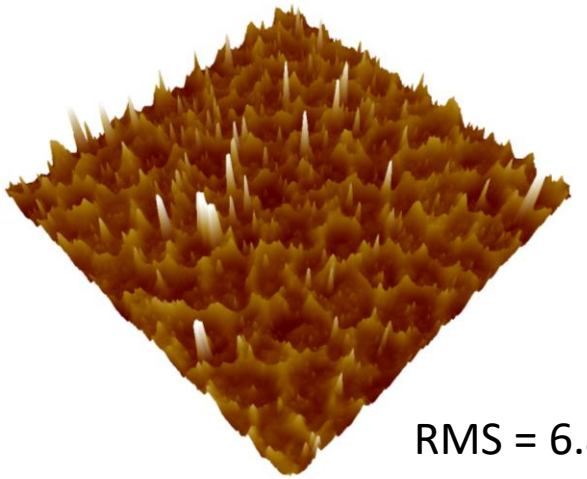

RMS = 6.8 nm

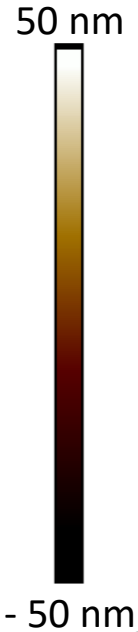

Secondary Ion Mass Spectrometry (SIMS)

d = 1 μm

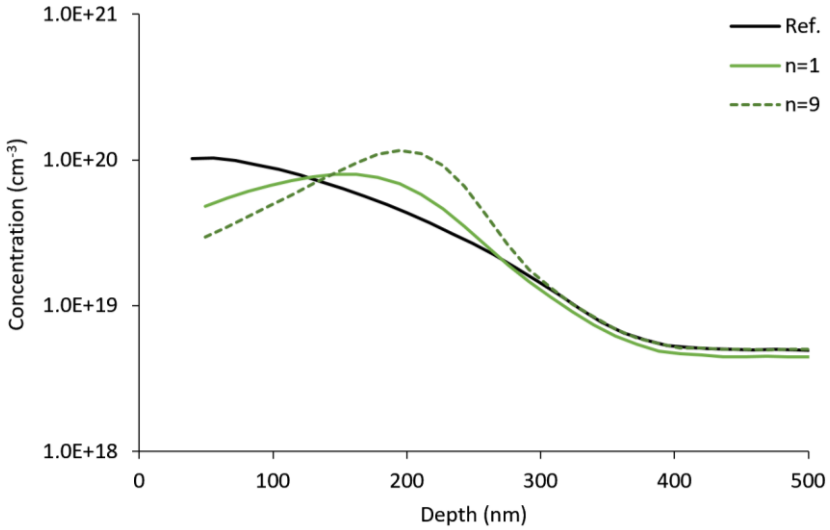

d = 2 μm

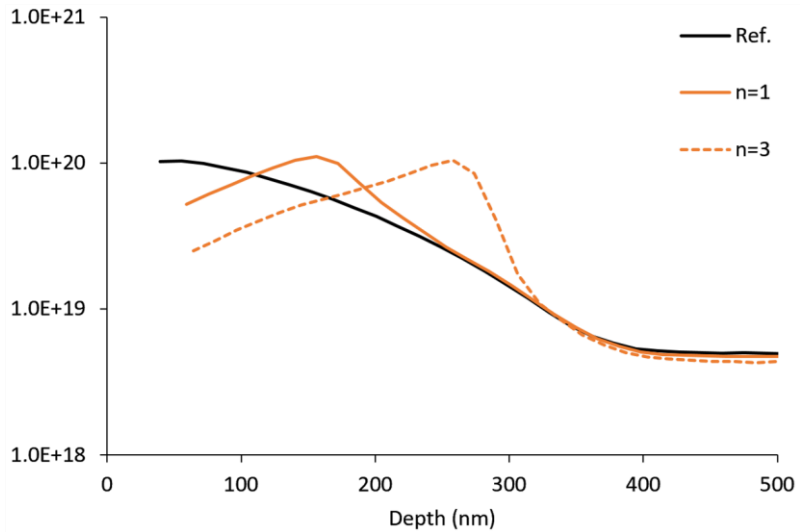

d = 3 μm

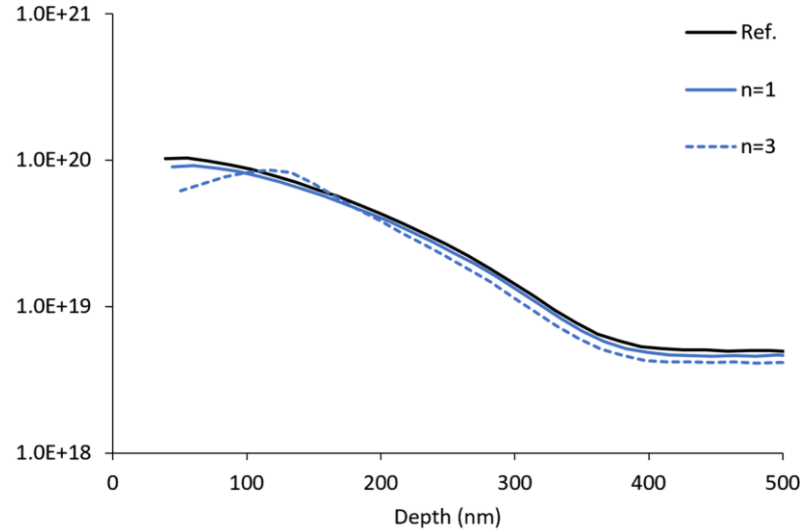

Laser pulse energy	E_P = 40 μJ
Laser line spacing	D = 10 μm

Observation and modelling of Boron pile-up in c-Si laser doping, due to Boron segregation coefficient >1

Lill (2017) *Boron Partitioning Coefficient above Unity in Laser Crystallized Silicon*. Materials (Basel) 10:189.

Conclusions

- Laser interaction with emitter (p++/p+ wafer) is weaker than on p-type wafer
  - Morphology compared by SEM
- Boron pile-up observed as reported in literature
- Laser spot overlap between pulses is fundamental to
  - Surface film morphology, and
  - And doping profile
- Future questions
  - Is it possible to melt the c-Si and still maintain a flat surface?
  - What will the doping profile of P be on the emitter (p++/p+ wafer)?

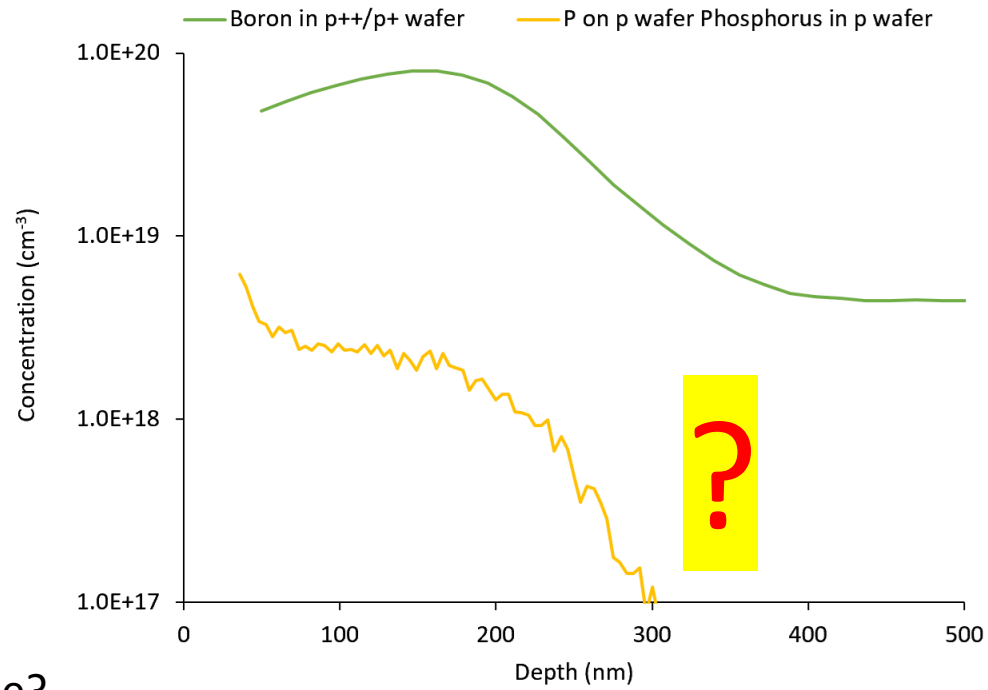

Laser doping and characterisation


Dr Filipe C. Serra


Afonso Guerra


Dr Guilherme Gaspar


Prof Killian Lobato

SIMS


Prof Lasse Vines

AFM


Prof Ana S. Viana

Support team

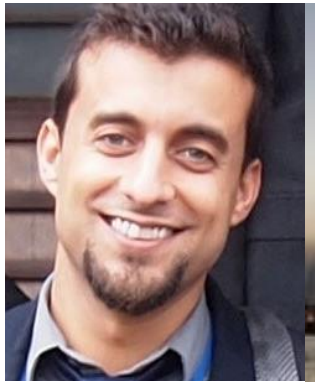
Dr David M. Pêra

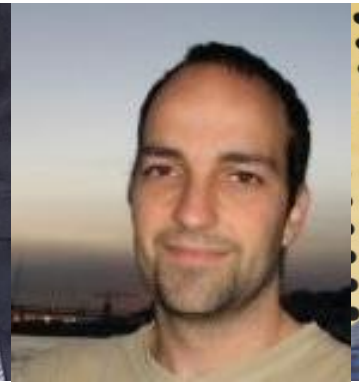
Dr Ivo Costa


Dr José M. Silva


Prof João A. Serra

Wafers


Dr Jayaprasad Arumughan

Ciências ULisboa
Faculdade de Ciências da Universidade de Lisboa

INSTITUTO DOM LUIZ

CQE Química Estrutural

UiO : University of Oslo

ISC International Solar Energy Research Center Konstanz

The Research Council of Norway

The S-LoTTuSS project was supported the Portuguese Science and Technology Foundation (FCT) through the grant agreements PTDC/CTM-CTM/28962/2017, PTDC/CTMCTM/28860/2017, 02/SAICT/2017 Nº 02883, UIDB/00100/2020-CQE and UIDB/50019/2020 – IDL financed by national funds FCT/MCTES (PIDDAC), and supported by The Research Council of Norway (RCN) through Project No. 239895/F20.

FCT Fundação para a Ciência e a Tecnologia
MINISTÉRIO DA CIÊNCIA, TECNOLOGIA E ENSINO SUPERIOR

We are hope to see you, in person, soon!

materials such as TCOs and perovskite ETLs and HTLs, even on textured bottom cells, and does not require the very long plasma-depositions needed to grow the nc-Si(p^+)/nc-Si(n^+) stacks.

De Bastiani (2020) Recombination junctions for efficient monolithic perovskite-based tandem solar cells: Physical principles, properties, processing and prospects. Mater Horizons 7:2791–2809.

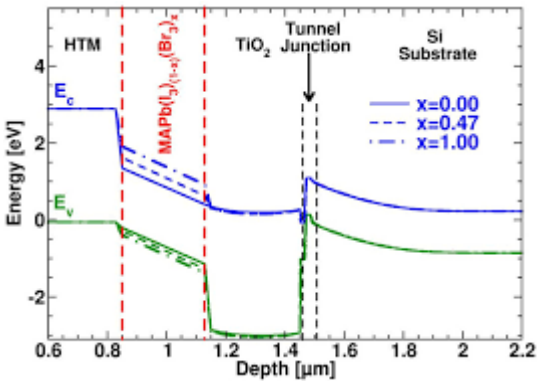

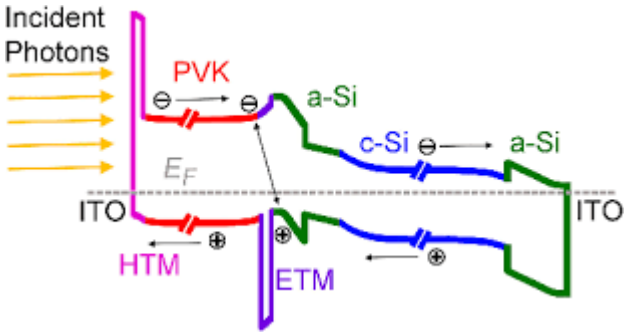

TCO has high lateral conductivity which imposes constraints due to shunting.

TCO causes parasitic absorption due to free carriers – free carrier absorption-FCA (which can also lead to some unwanted device heating)

nc-Si tunnel junctions are slow to grow.

This is where laser processing can come it.

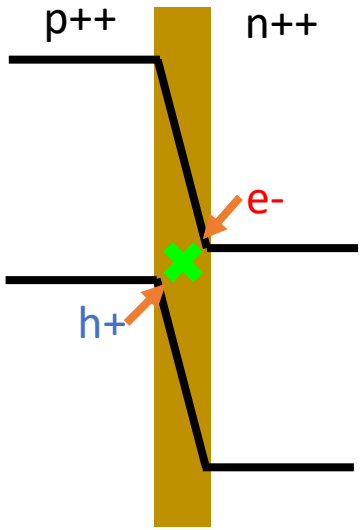
p++
n++
e-
h+

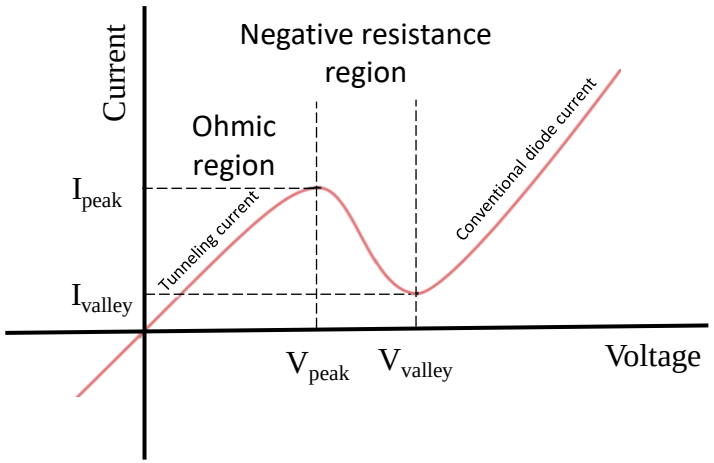
Current
Negative resistance region
Ohmic region
I_{peak}
I_{valley}
Tunnelling current
Conventional diode current
V_{peak}
V_{valley}
Voltage

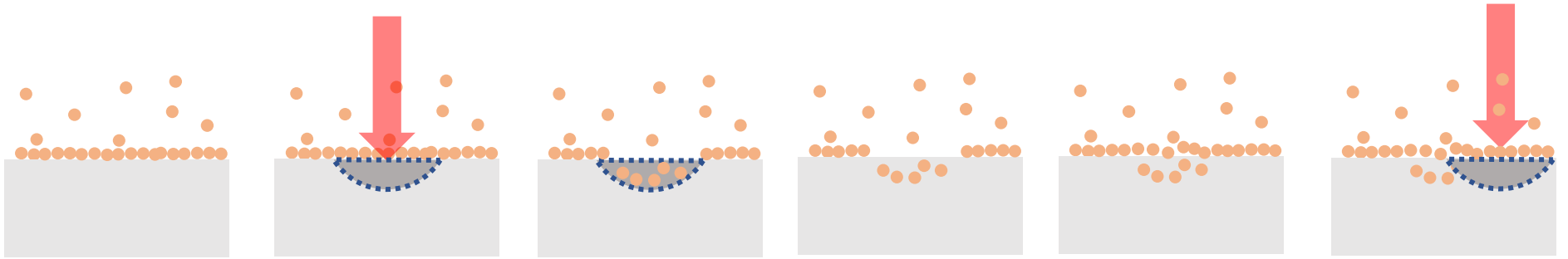

1. immersion

2. Laser pulse & melting

3. Dopant diffusion in melt

4. recrystallization

5. Dopant adsorption

6. Laser pulse +(x,y)

Sequential pulsing = **higher doping**

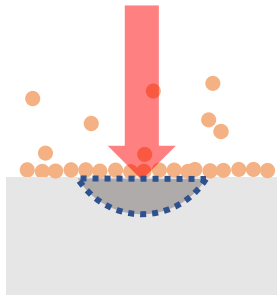

Laser pulse & melting

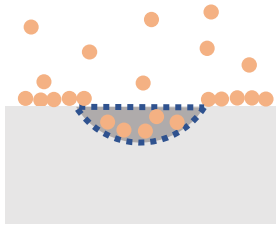

Dopant diffusion in melt

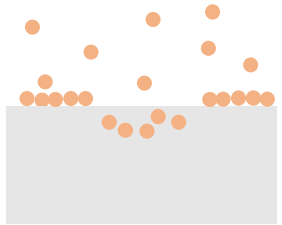

recrystallization

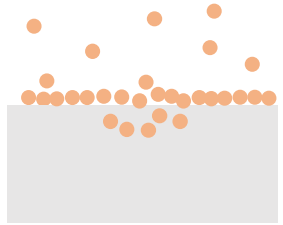

Dopant adsorption

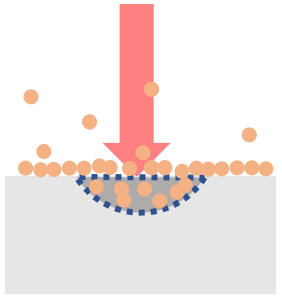

Laser pulse & melting

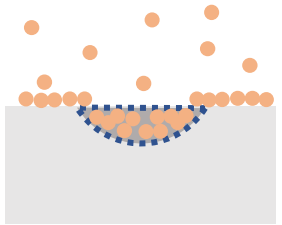

Dopant diffusion in melt

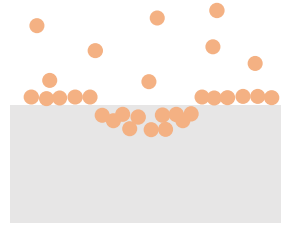

recrystallization

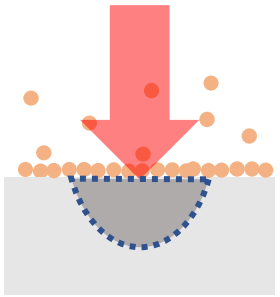

Laser pulse & melting

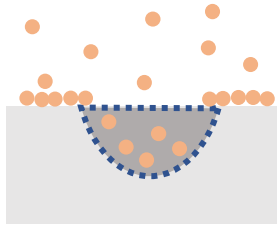

Dopant diffusion in melt

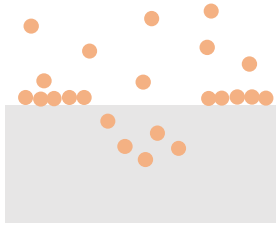

recrystallization

Higher pulse energy = deeper melt = **deeper doping**

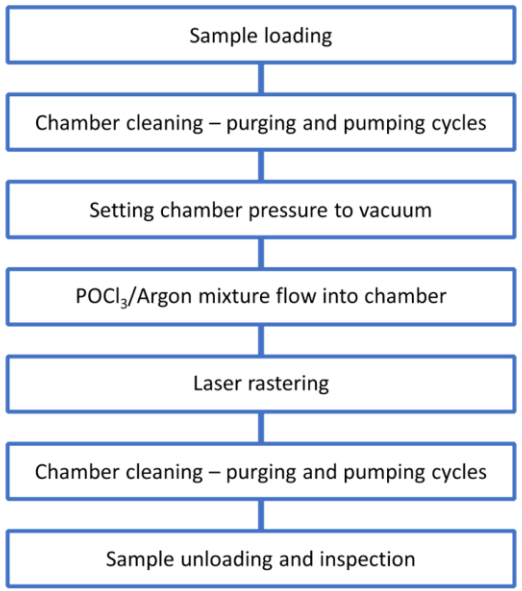
Sample loading
Chamber cleaning – purging and pumping cycles
Setting chamber pressure to vacuum
POCl3/Argon mixture flow into chamber
Laser rastering
Chamber cleaning – purging and pumping cycles
Sample unloading and inspection

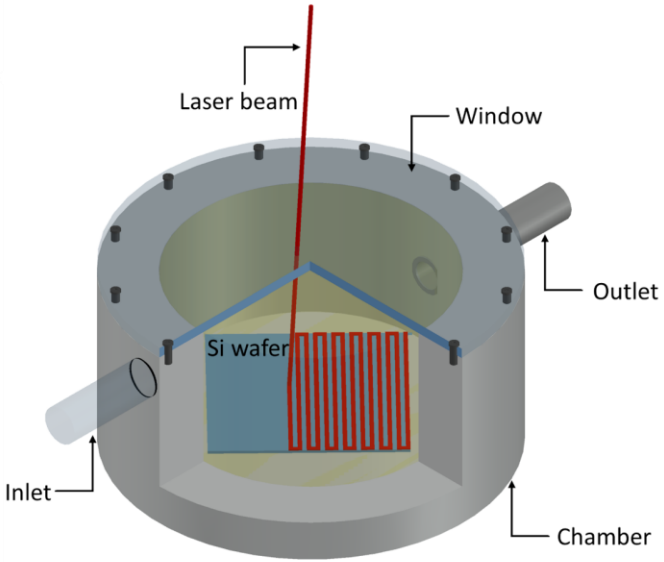
Laser beam
Window
Outlet
Si wafer
Inlet
Chamber

Start with standard wafer with a p+ emitter

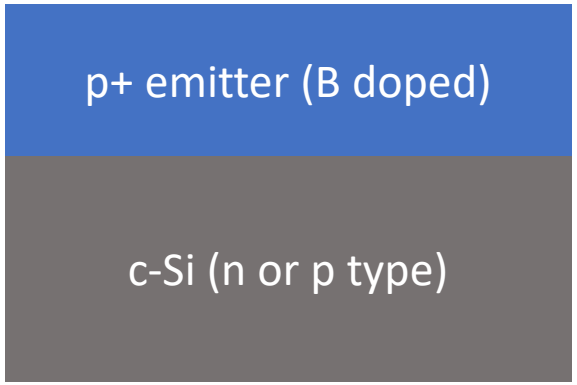

n++ dope the emitter

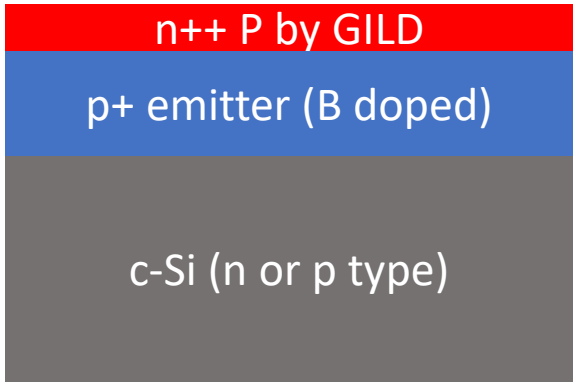

To form n++/p+ tunnel junction

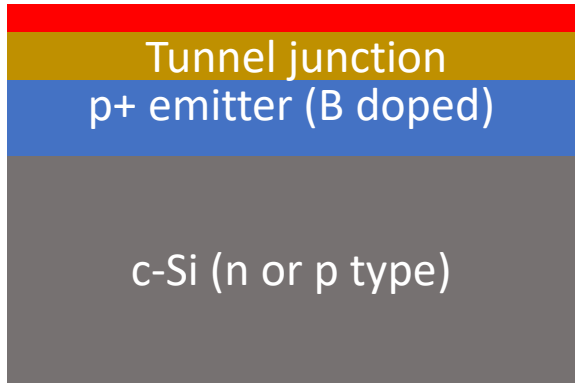

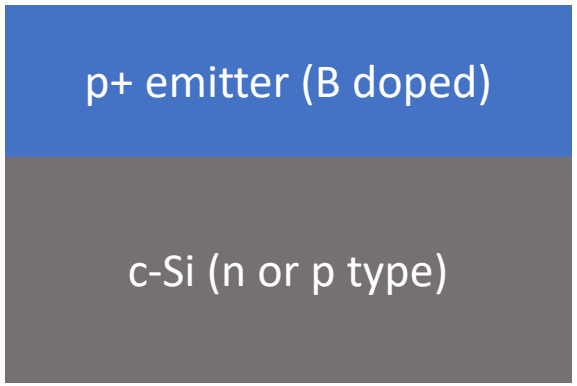

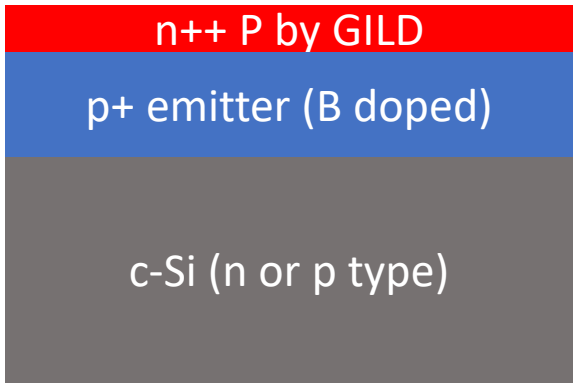

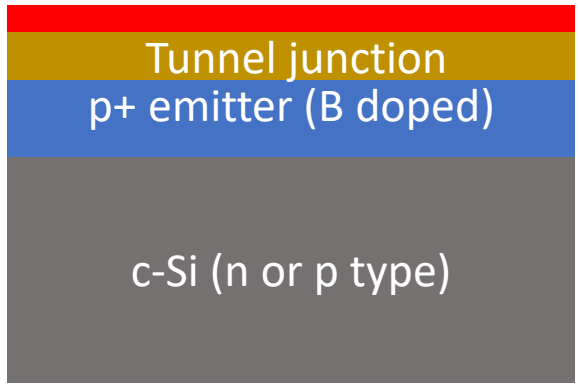

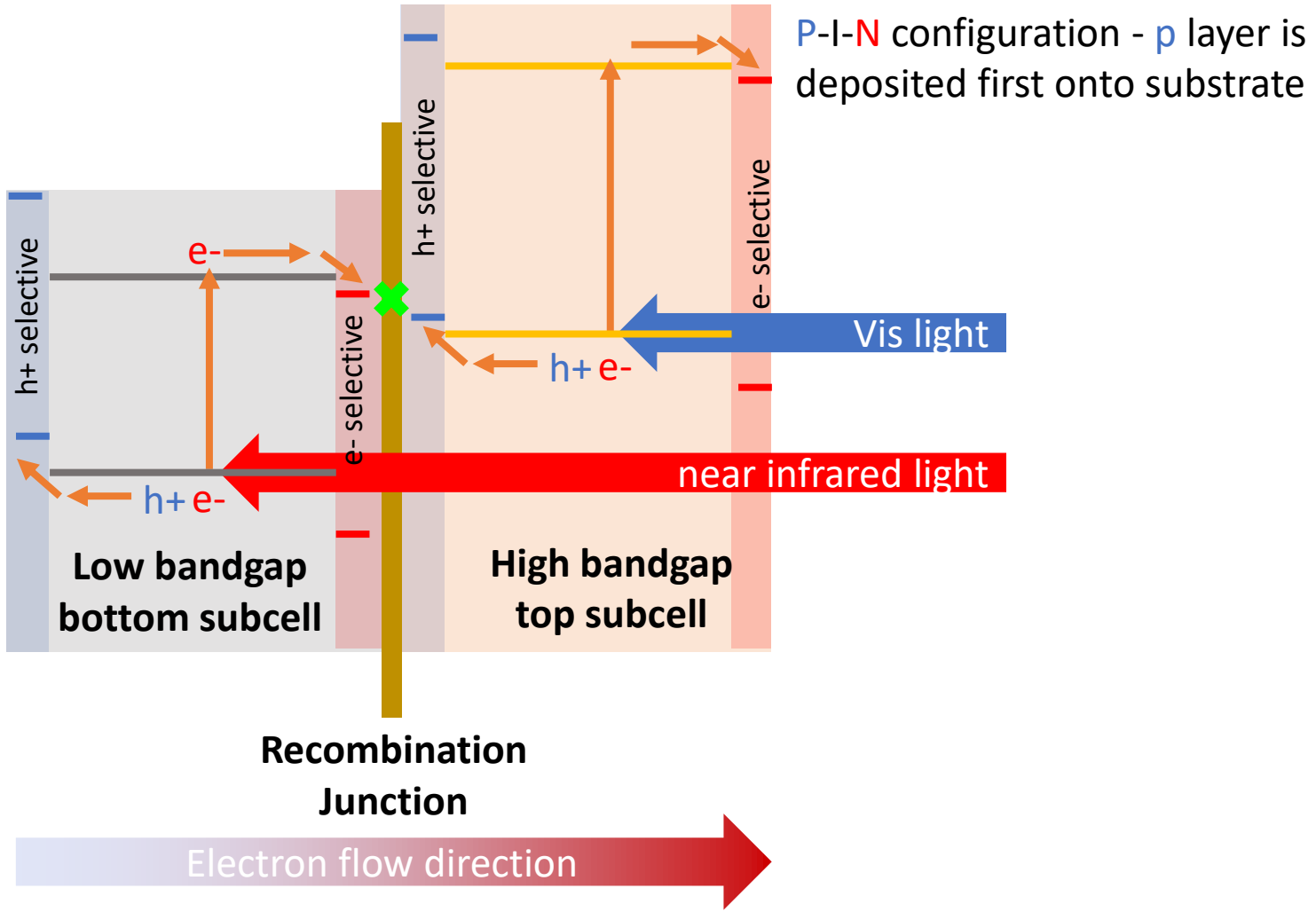
P-I-N configuration - p layer is deposited first onto substrate
h+ selective
e- selective
h+ selective
e- selective
e-
h+ e-
h+ e-
Vis light
near infrared light
Low bandgap bottom subcell
High bandgap top subcell
Recombination Junction
Electron flow direction

1.1 Perovskite on silicon tandem solar cells

- Current flow is determined by placement of selective contacts.

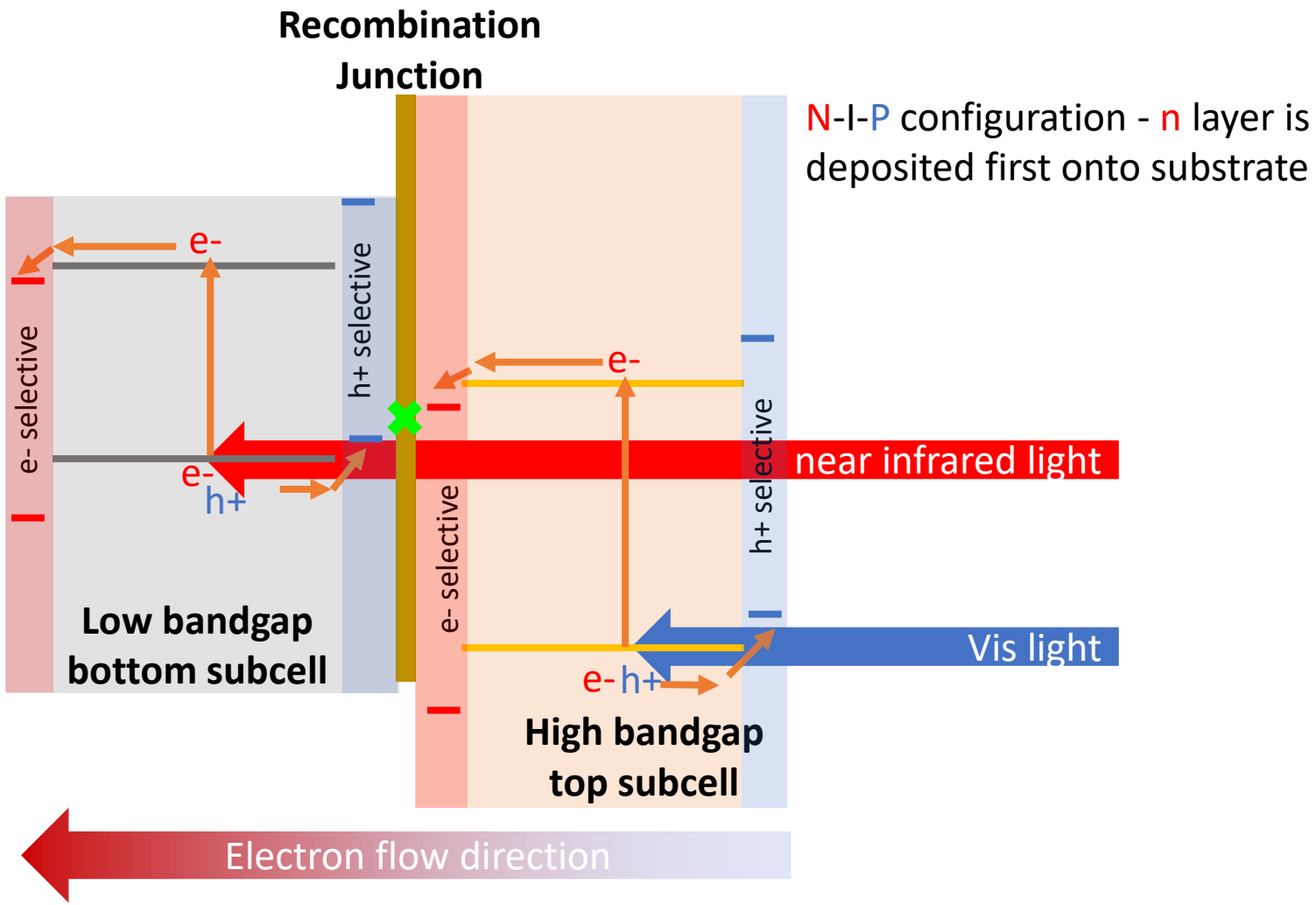

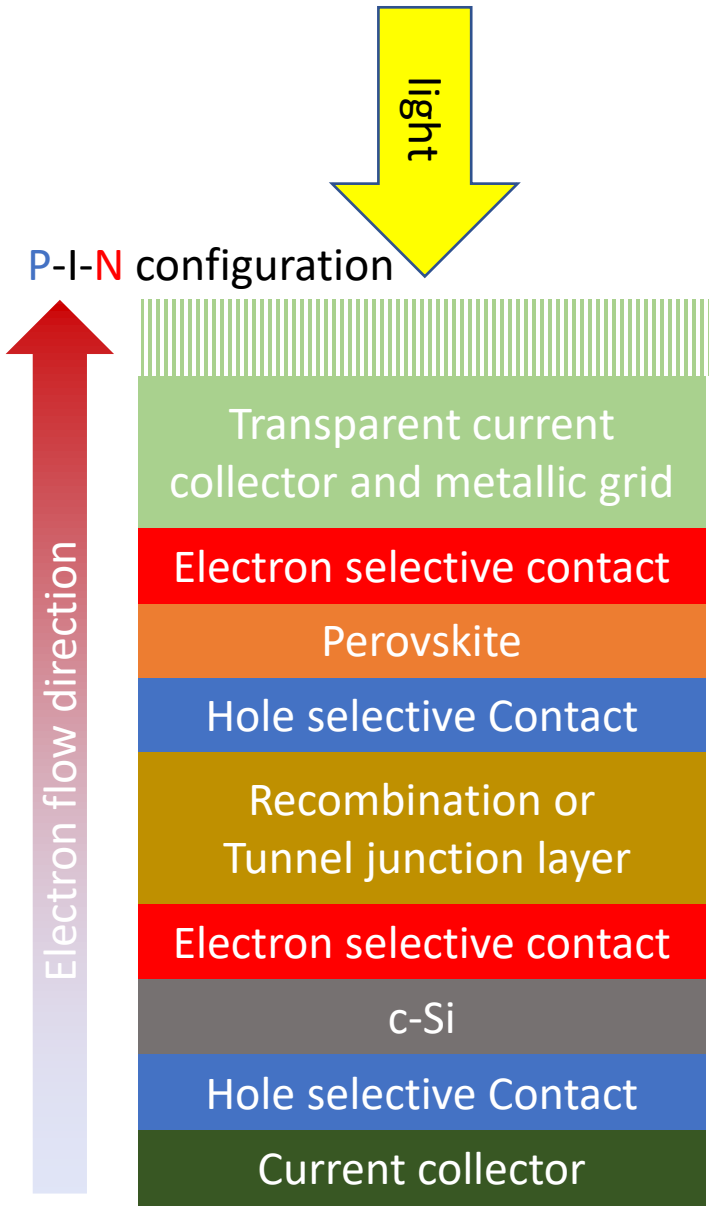
light
P-I-N configuration
Electron flow direction
Transparent current collector and metallic grid
Electron selective contact
Perovskite
Hole selective Contact
Recombination or Tunnel junction layer
Electron selective contact
c-Si
Hole selective Contact
Current collector

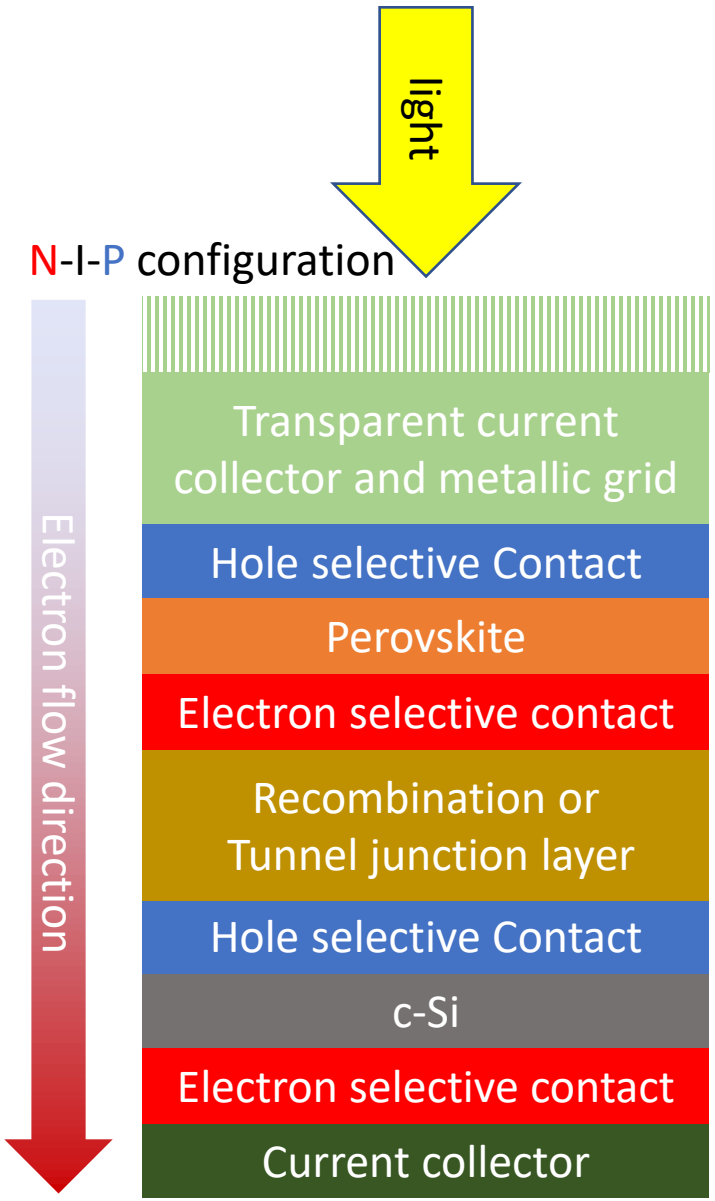
light
N-I-P configuration
Electron flow direction
Transparent current collector and metallic grid
Hole selective Contact
Perovskite
Electron selective contact
Recombination or Tunnel junction layer
Hole selective Contact
c-Si
Electron selective contact
Current collector

P on p wafer - Vary number of passes
E_pulse=40microJ, D_line=10micron, F=500KHz, Waveform=0,
d=2micron

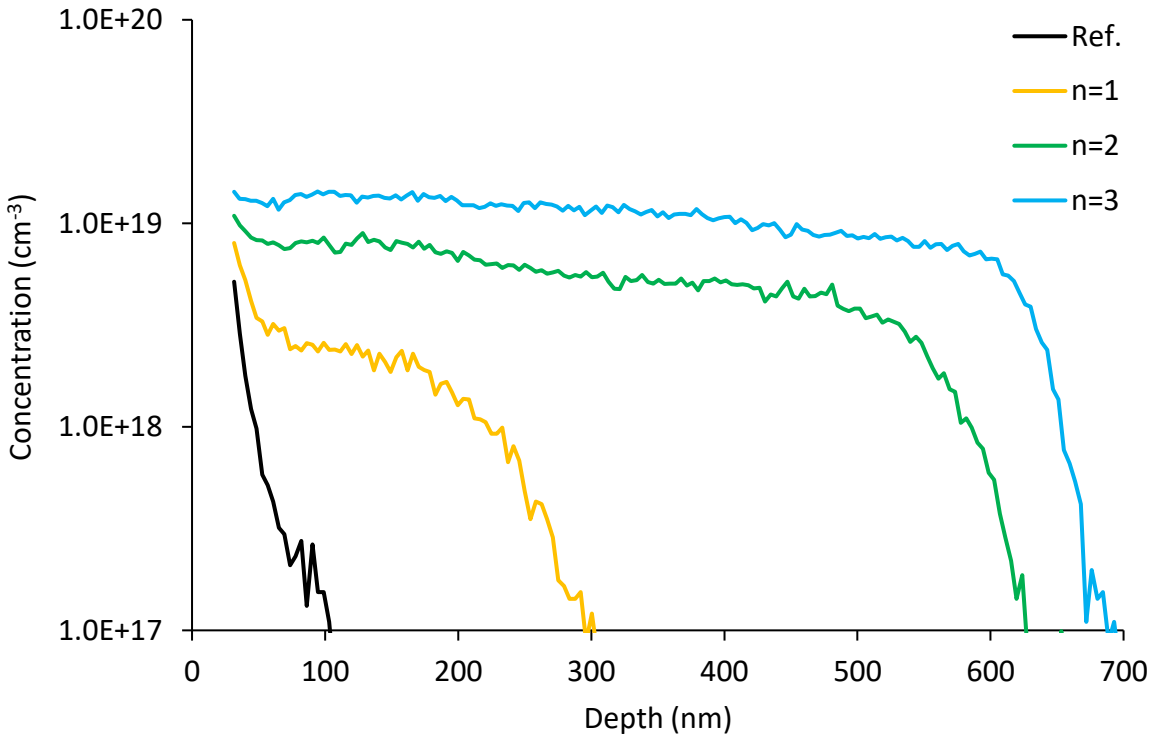

P on p wafer - Vary number of passes
E_pulse=40microJ, D_line=10micron, F=500KHz, Waveform=0,
d=1micron

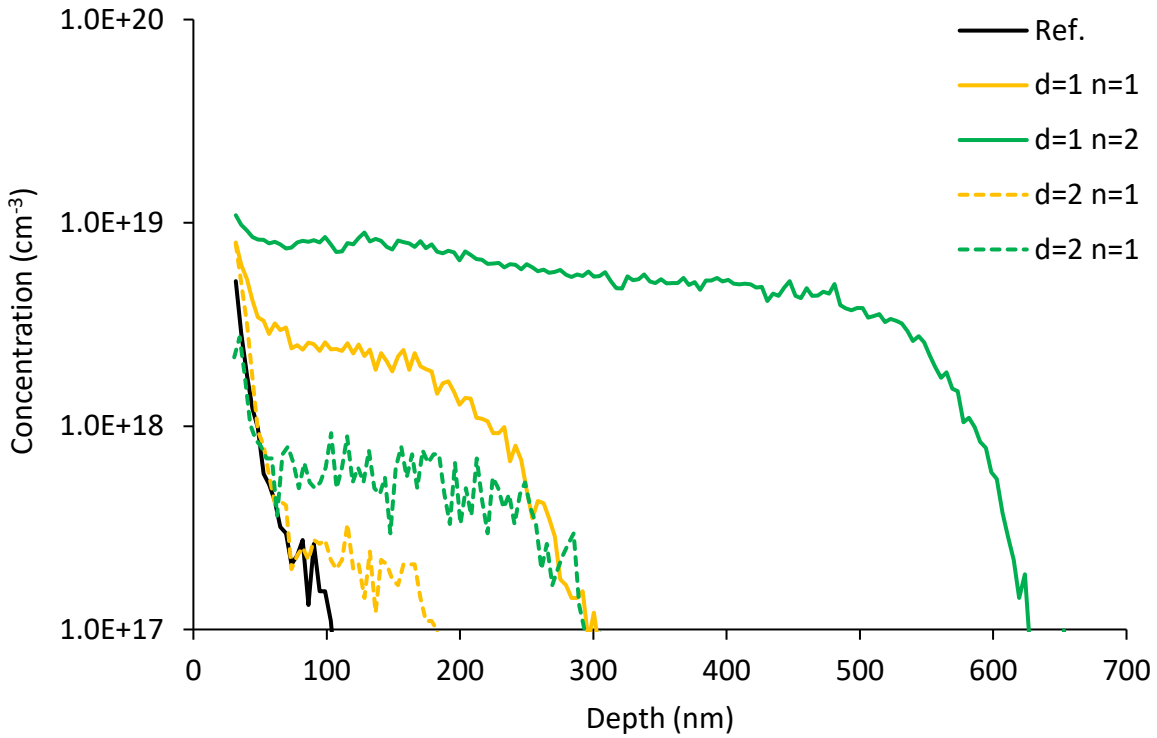

Vary number of passes
E_pulse=40microJ, D_line=10micron, F=500KHz, Waveform=0,
d=1micron

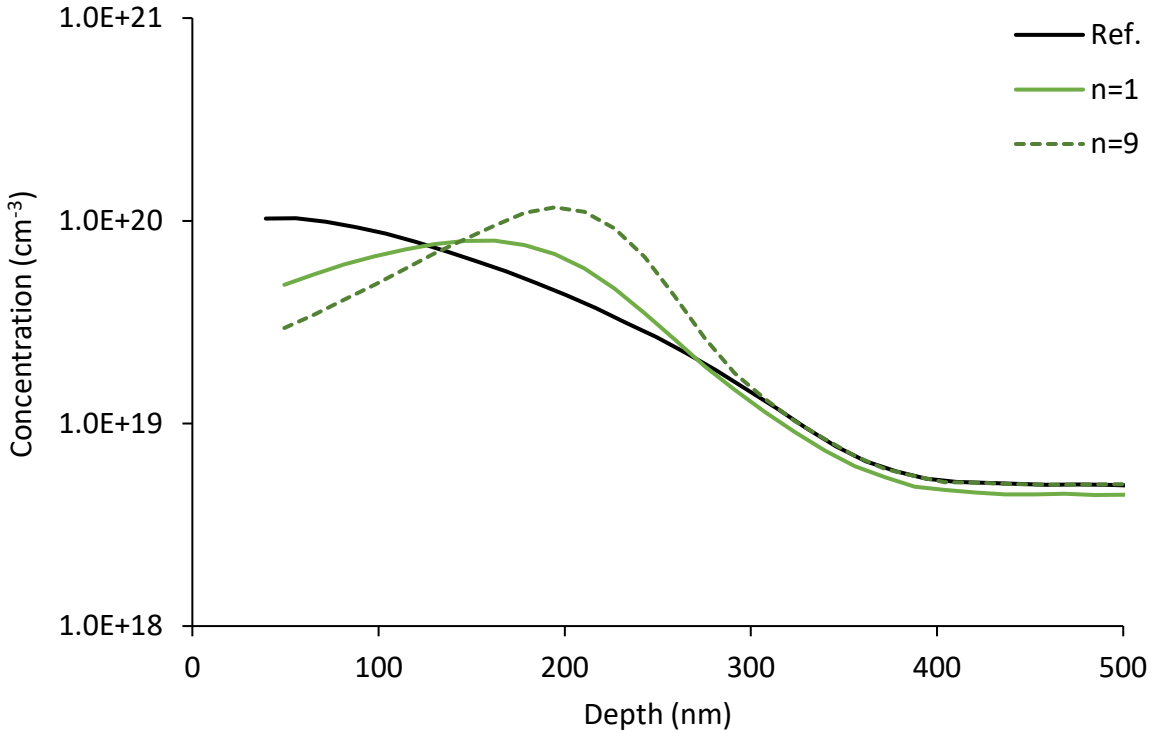

Vary number of passes
E_pulse=40microJ, D_line=10micron, F=500KHz, Waveform=0,
d=2micron

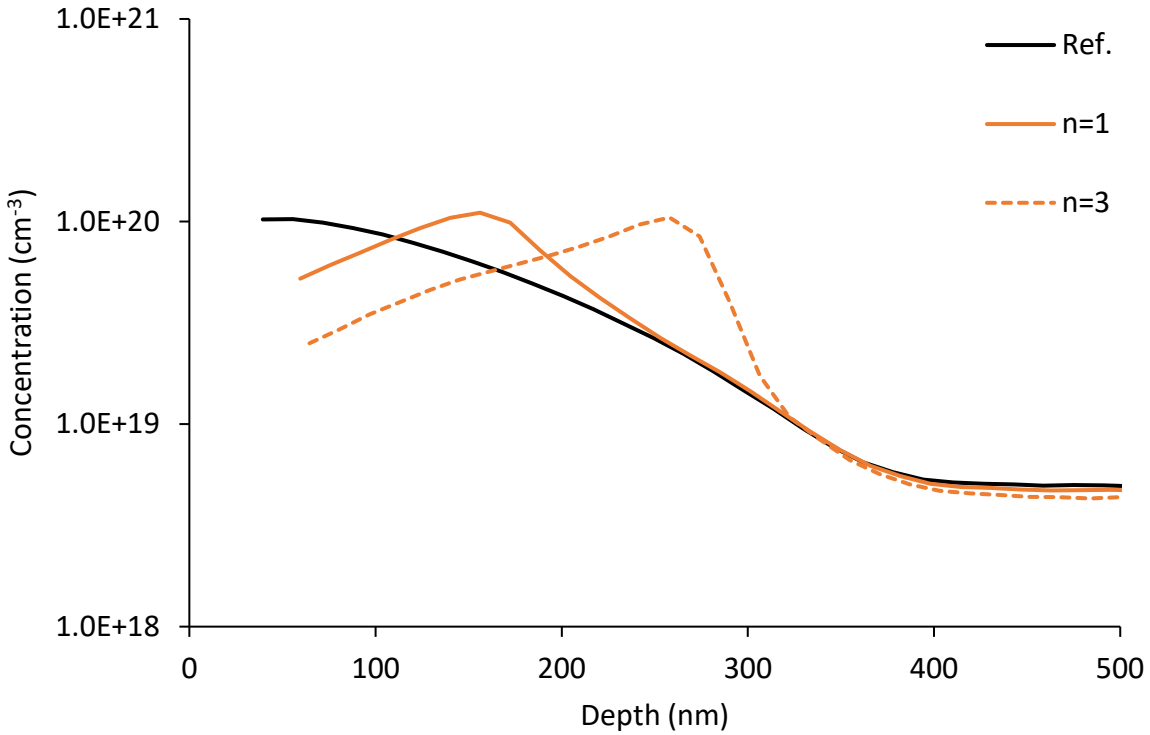

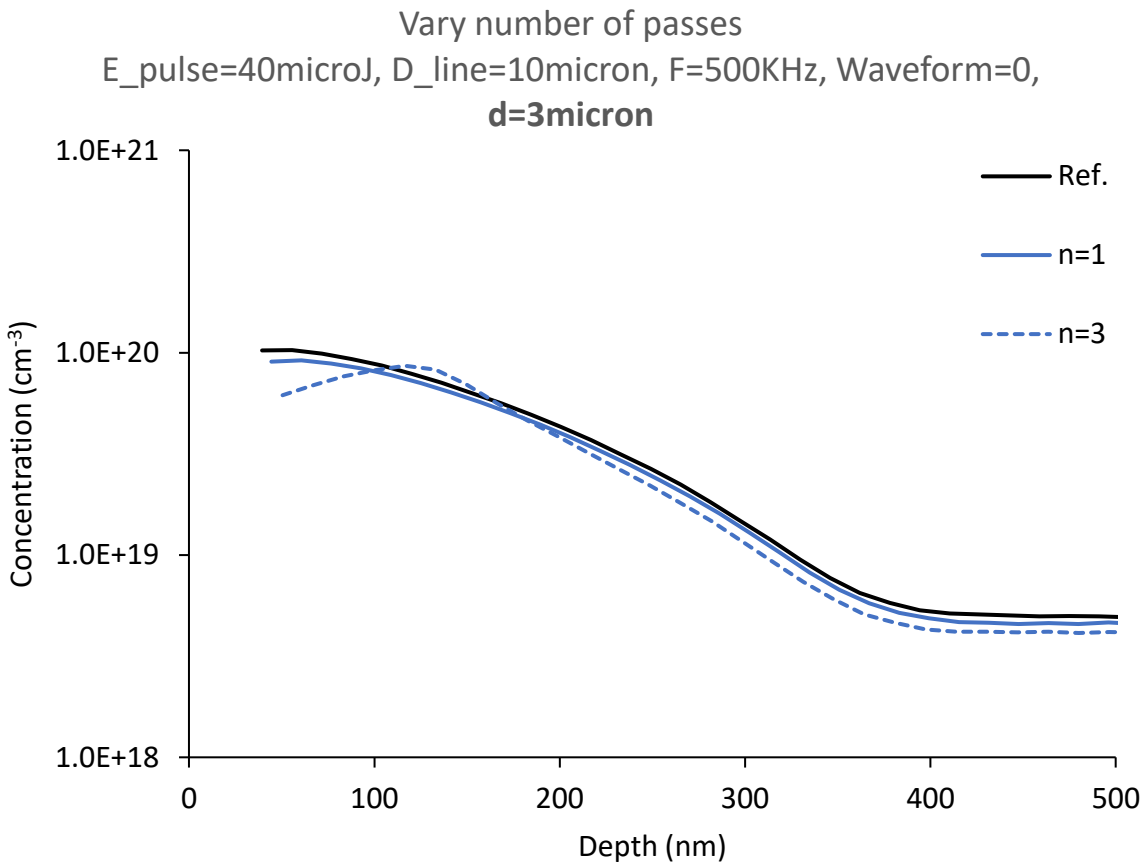
Vary number of passes
E_pulse=40microJ, D_line=10micron, F=500KHz, Waveform=0,
d=3micron
1.0E+21
1.0E+20
1.0E+19
1.0E+18
Concentration (cm-3)
0
100
200
300
400
500
Depth (nm)
Ref.
n=1
n=3

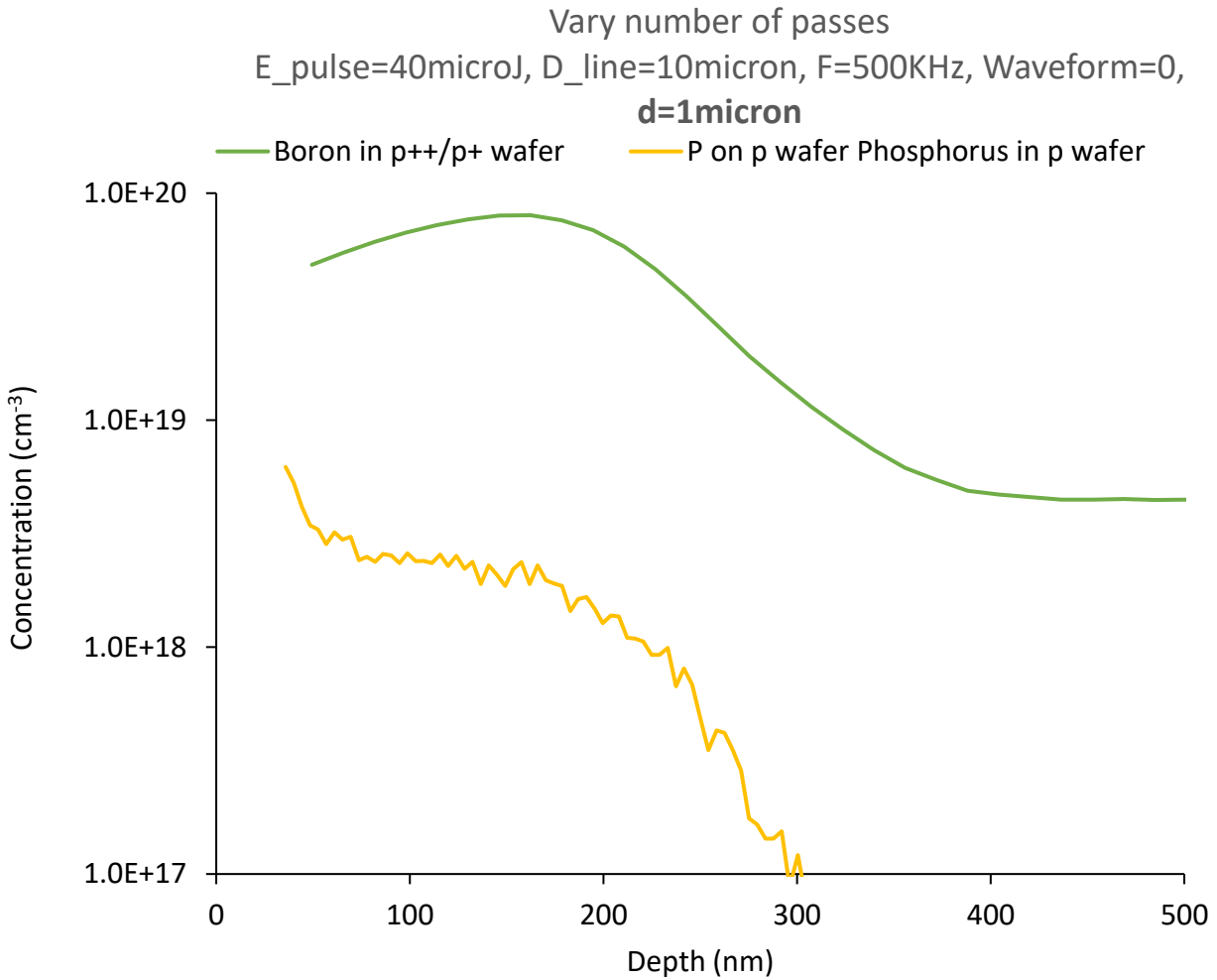
Vary number of passes
E_pulse=40microJ, D_line=10micron, F=500KHz, Waveform=0,
d=1micron
Boron in p++/p+ wafer
P on p wafer Phosphorus in p wafer
1.0E+20
1.0E+19
1.0E+18
1.0E+17
Concentration (cm-3)
0
100
200
300
400
500
Depth (nm)